SMARTPHONE PLASTIC OPTICAL FIBER SENSORS

Arman Aitkulov, B. Eng

Submitted in fulfillment of the requirements

for the degree of Master of Science

in Electrical and Electronics Engineering

School of Engineering

Department of Electrical and Electronics Engineering

Nazarbayev University

53 Kabanbay Batyr Avenue,

Astana, Kazakhstan, 010000

Supervisor: Daniele Tosi

December 2018

Declaration

I hereby, declare that this manuscript, entitled “title of thesis”, is the result of my own work except for quotations and citations which have been duly acknowledged.

I also declare that, to the best of my knowledge and belief, it has not been previously or concurrently submitted, in whole or in part, for any other degree or diploma at Nazarbayev University or any other national or international institution.

Name: Arman Aitkulov

Date: 15.12.2018

Abstract

Telehealth is quickly becoming an essential tool in delivering medical care. It can easily be used to monitor the states of patients who are located at remote locations away from hospitals. For example, breathing rate is one of important physiological parameters requiring monitoring, since it can be used in the diagnosis of respiratory diseases. However, the tools of remote monitoring have to be cheap and easy in use. These requirements can be satisfied by smartphone sensor based on plastic optical fiber (POF). The proposed solution is an all-fiber sensor where the flashlight acts as a light source and the camera acts as a photodetector. First of all, smartphones have become ubiquitous. POF, on the other hand, is not expensive. Hence, the proposed combination can be a cost-effective solution for implementing telehealth. In the work, the technique of intensity modulation in POF is adapted for sensing breathing rate. The measurements are analyzed in both time and frequency domains. In addition, multiplexing is also a promising direction for conducting sensing in optical fibers, since it can be used to measure multiple parameters. The possibility of implementing it in POF will be considered as well.

Table of Contents

List of Abbreviations and Symbols

BFB	bifurcated fiber bundle
COPD	chronic obstructive pulmonary disease
FFT	fast Fourier transform
FBG	fiber Bragg gratings
GOF	glass optical fiber
H_2S	hydrogen sulfide
He-Ne	helium-neon
LED	light emitting diode
MRI	magnetic resonance imaging
NA	numerical aperture
PCS	plastic cladded silica
PLA	polylactic acid
PMMA	polymethyl methacrylate
POF	plastic optical fiber
RI	refractive index
SLED	superluminescent diode

List of Tables

List of Figures

Chapter 1 – Introduction

Biophysical parameters have a great significance in medicine as a basis for diagnoses, a reasoning for preventive steps or a tool for monitoring healing processes. For example, bending of lower back is an indicator crucial in identifying the causes of back pain and avoiding serious health problems [1]. Joint movements often need to be monitored during physical therapies [2]. Breathing rate is also very important as a parameter used in recognizing deviations from normal patterns of respiration and registering conditions that can lead to respiratory diseases. For instance, chronic obstructive pulmonary disease (COPD) is a widespread breathing problem that requires continuous monitoring to avoid possible exacerbations. One of the signs indicating the worsened state of a patient diagnosed with COPD is an increase in respiration rate [3]. If this rise in breathing intensity is registered several days in advance, necessary preventive methods such as hospitalization can be taken at the right time to avoid further complications. Moreover, an increase in frequency of breathing movements can indicate the risk of cardiac arrest [4]. Due to the importance of breathing activity, it is going to be the focus of this thesis.

Considering the current trends in population growth, there are more people who require health monitoring [5]. One of the ways to meet these needs is to utilize the tools of telehealth that applies computing techniques in conjunction with communication systems to provide people with remote health monitoring [6]. The advantages of the method include cost-effectiveness, comfortable home conditions for patients and ability to provide monitoring on a daily basis or over long periods of time. Remote monitoring can also be used to alarm medical personnel in case of emergency situation. In addition, telehealth can serve as an alternative to medical checkups in the remote areas where people

do not have regular access to services usually provided by hospitals [7]. Moreover, the approach is becoming more widespread due to the advances in communication and computing capabilities.

The requirements of implementing telehealth and remote monitoring include low cost and possibility to be used in home conditions. This is why smartphones are considered to be a viable tool for the applications in this area, since they have become widely available. Other advantages of the remote monitoring implemented by smartphones include the rise in the efficiency of the mobile hardware and the ease of use. In addition to providing communication channels [8], smartphones are also capable of collecting and processing information related to the states of patients under monitoring. For instance, there are smartphone accelerometers which can track movement. Smartphone cameras are also an essential tool in the implementation of various sensors. It was shown that pulse can be counted by smartphone camera through observing changes in the skin color of fingertips [9]. The combination of smartphone camera and LED was also used to differentiate between the frequencies of heart beatings associated with different emotional states [10].

However, the architecture of smartphone requires some modifications in order to track physiological parameters discussed earlier. In the current work, the combination of smartphones and plastic optical fiber (POF) is going to be explored. POF fulfills the requirement of cost-effectiveness. Its compact and lightweight characteristics are a perfect fit for sensing applications in home conditions. As a part of curvature sensor, it can be applied in non-invasive way, increasing the level of comfort for patients. Moreover, due to the recent developments, POF has become a viable alternative to glass optical fiber (GOF). One of the popular techniques in POF-based sensors is intensity modulation. It uses POF as a propagating link between light source and photodetector. The

modulation of displacement can be used to make POF sensitive to breathing. Intensity modulation is a good fit for applications in smartphones, since its flashlight and camera can be used to provide input and read output, respectively. Multiplexing is also a promising direction in the area of sensors, since it can be used to collect information about several parameters [11].

The purpose is to develop a cost-effective and compact sensor that can measure frequency of breathing. The work marks the first time the combination of POF and smartphone is used to monitor breathing rate. In order to do that, several objectives have to be fulfilled:

1) It needs to be shown that POF can provide a sufficient level of sensitivity for such application. An important tool in the sensor is a coupler connecting POF and smartphone. It will be 3D-printed.

2) The experiments showing that frequency of breathing can be extracted by POF-based sensor have to be conducted.

3) Then, the method of collecting data through the smartphone architecture has to be developed. It is going to be implemented by a specifically developed Android application.

In addition, the possibility of multiplexing several POFs with smartphone is going to be explored. The core of POF will be tested as a curvature sensor.

The next chapter is literature review, where several papers that helped to choose the methods applied in the work are considered. Previous works on optical sensors are evaluated. Then, the methodologies behind each component of the sensing system are explained. Following this, the simulations are conducted to obtain some theoretical expectations. Then, the results of implementing the sensors are compared with the simulations. After that, the measurements of breathing and the experiments on multiplexing are discussed.

Chapter 2 – Literature review

2.1 Optical fiber technology and sensing methods based on it

Firstly, the theoretical background behind POF needs to be considered. It includes a discussion on advantages and disadvantages associated with the transmission properties of POF, as well as some information on light propagation inside optical fibers. In addition, different sensing paradigms that can be implemented by POF are reviewed.

The review made by Polishuk [12] emphasized the benefits of using POF instead of its alternative, GOF. Industries had usually preferred GOF due to its lower attenuation rates. It can allow a loss of only 0.2 dB/km, while POF made of polymethyl methacrylate (PMMA) has an attenuation rate of 150 dB/km. However, the issue of attenuation is a serious concern when long distances are involved. The advantages of POF become more evident in applications requiring transmission over short distances, such as sensors. POF operates in a visible light; it is also cheaper, lighter and easier in handling and coupling due to larger dimensions. Moreover, POF can work in conjunction with a simple light emitting diode (LED), while GOF requires laser light to be transmitted. The limitations of the attenuation over distance are possible to be overcome by using perfluorinated polymers. However, the performance of POF degrades under exposure to high temperatures.

Figure 2.1: Schematic of intensity modulation [13]

The paper by Bilro et al. [13] further elaborated on the increasing interest in POF and the advantages of such fibers over other alternatives. They are

highly flexible and robust under industrial conditions. However, the limiting temperature for the proper operation of POF is 100°C. Higher temperatures can lead to the fiber losing its robustness. Enhanced types of polyethylene can increase the limit to 135°C. The authors considered essential sensing techniques that can be implemented by POF, mainly intensity modulation. It is a simple and wide-spread method. The basis setup includes light source and photodetector in addition to the POF link connecting them. As a result of attenuation caused by external factors such as Rayleigh scattering, absorption, macro- or microbending, the propagating properties of POF degrade and the amount of power received by photodetector changes. The schematic representation of the method is shown in Figure 2.1. The method of path difference was discussed as well. The same signal propagates through two fibers; the first one is used as a reference while the second one experiences deformations due to interactions with the surrounding environment. Then, the phases of the two output signals are compared, and the conclusions about the external impact can be made.

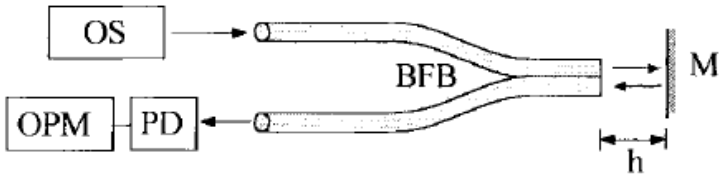

Figure 2.2: Transmission between two fibers through mirror [14]

Although POF was not the subject of discussion in the paper by Faria [14], the theoretical analysis conducted by the author was very helpful in understanding the propagation of light inside optical fibers in terms of geometrical relationships. An optical displacement sensor based on a configuration known as bifurcated fiber bundle (BFB) was considered. BFB is a setup where two fibers are aligned side by side on one end and split on the other one, as seen in Figure 2.2. At the splitting end, one of the fibers is connected to light source and the second fiber is connected to photodetector. Mirror is placed

next to the combined parts of the fibers. It is used to direct light from the transmitting fiber to the receiving one. Such arrangement is known as the reflection scheme, in contrast to the direct transmission scheme shown in Figure 2.1. The dependence of the received light on the distance from the fibers to the mirror was derived using geometrical rules; the resulting relationship is shown in Figure 2.3.

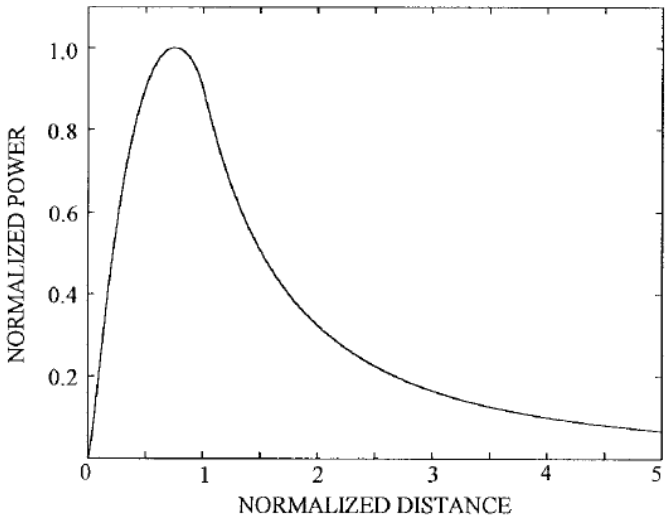

Figure 2.3: Dependence of the received intensity on the displacement between the fibers [14]

The attractive characteristics of POF in the context of the intensity modulation scheme were further demonstrated by Yang et al. in the review paper [15]. The low cost of manufacturing and portability make POF-based sensors a viable option in comparison with the already existing types of detectors. POF also has a high numerical aperture (NA), which means that it can receive light incoming at a wide range of angles, and a relatively large radius. This is why it is easy to couple light into POF. It was stated that the sensitivity of the fiber could be amplified by increasing the radius, but the linear range of POF would be diminished. The authors noted that the proper functioning of POF is directly linked to the amount of noise contributed by a surrounding environment. A yellow helium-neon (He-Ne) laser light operating at 594 nm

was recommended as the source in order to achieve higher sensitivity. The paper indicated that the further studies need to pay attention to the stability of the light source, because fluctuations can have an impact on the quality of sensing activity.

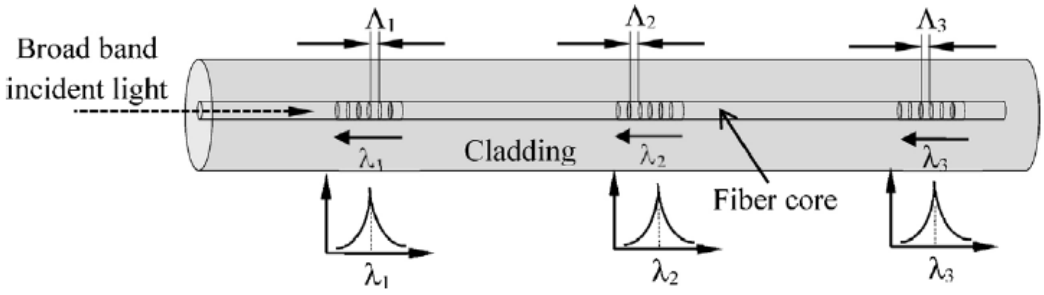

Figure 2.4: Scheme of the FBG method [16]

Cheng-Yu et al. provided an extensive overview of the sensing method based on FBG [16]. According to the sensing principle, the structure of the fiber core is modified by spatially periodic gratings which signify changes in the refraction index. As a result, when light is coupled into the fiber, specific wavelengths are reflected by these gratings and the rest are transmitted. For example, each grating can be chosen in a way that allows it to reflect a certain wavelength depending on a level of temperature or an applied strain. The schematic of the method is shown in Figure 2.4.

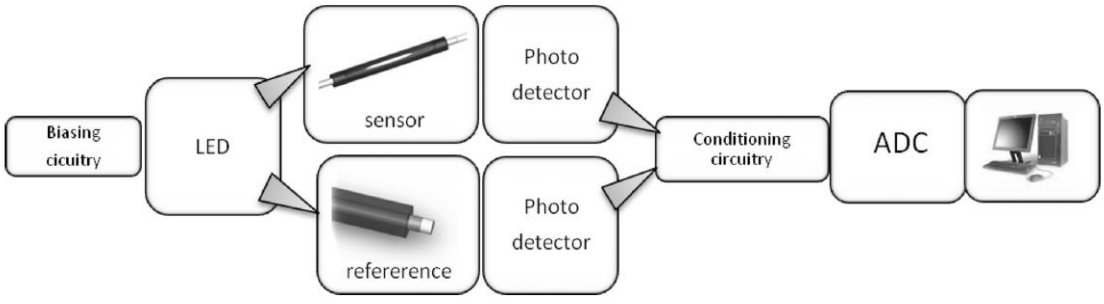

Figure 2.5: Sensing setup based on path difference [17]

Another research by Bilro et al. [17] demonstrated a sensing method for detecting the refractive index (RI) of a surrounding medium. The light was transmitted through 2 fibers; the first one was used for sensing and the second

one was used as a reference, as shown in Figure 2.5. Then, the output signal was normalized with respect to the reference. It was stated that in order to make POF more sensitive, its transmission properties need to be weakened. One of the ways to accomplish that is to expose the fiber core by side polishing, which is simple in the case of POF. The side polished region of POF was successively immersed into solutions with different concentrations of water and glycerol. Different amount of light was delivered depending on the RI of a solution being measured. However, low sensitivity was registered for the RI values lower than 1.4. In addition, the authors implemented a sensor for measuring curvature. In POF, NA is about 0.5, which means that it has more than 2 million ways for light to propagate along. When macrobending is applied to the exposed core of POF, its NA is reduced. Therefore, less light is able to be transmitted through the fiber core. Distinct intensities were detected for different curvature radii. The experiments were conducted using an LED with center wavelength of 660 nm and a data acquisition board connected to PC for collection of measurements from photodiodes. After testing the sensors independently, they were combined for simultaneous detection of RI and curvature. The same deformations were applied to the fiber for each solution of glycerol and water. For the cases when the RI of the solution was lower than 1.4, the plots of the received intensity vs. curvature radius were almost identical. It indicates low sensitivity, similarly to the part when the RI sensor was considered independently. However, the simultaneous measurements of RI and curvature are possible for the RI values higher than 1.4.

2.2 POF-based sensing applications

The following paragraphs mainly overview some of the applications for the sensors that utilize POF, mostly focusing on intensity modulation. Firstly, several possible applications of POF are reviewed. Then, the works focusing on

measuring breathing rate are discussed, followed by the implementation of multiplexing.

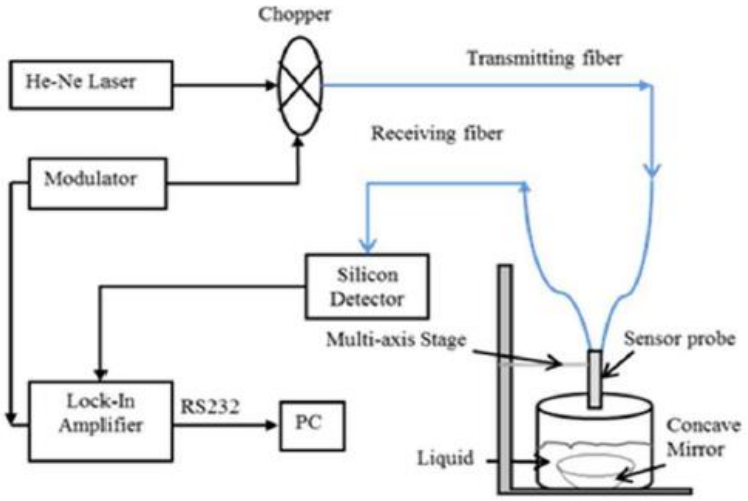

Figure 2.6: Setup for measuring liquid level [18]

Yang et al. also demonstrated an example of POF-based sensor for measuring liquid level [18]. Intensity modulation was also applied, but reflection of light was monitored instead of direct transmission. The setup was similar to the theoretical propagation scheme considered previously in the paper on BFB, but the mirror was placed on the bottom of a container filled with water, as shown in Figure 2.6. Depending on the level of water in the container, different amount of light is reflected into the receiving fiber. A He-Ne laser operating at 594 nm was used to provide the input. The original signal was also fed to a PC that processed the output from the receiving fiber. The signal from the receiving fiber was read by a silicon detector. A lock-in amplifier was used to filter the noise from the light source. Then, the output power was normalized with respect to the input. POFs had radii of 0.25 mm. The sensor was able to successfully detect the liquid level from 0 mm to 20 mm.

Harith et al. [19] demonstrated a sensor that used POF to measure relative value of humidity in a surrounding environment. In their work, the coating was replaced with the zinc oxide nanostructures doped with aluminum after etching

the fiber. Such coating can absorb water, changing the transmission properties of the fiber, such as its RI. It means that different humidity levels correspond to various amount of power at the output. A He-Ne laser at 633 nm was used as the input, and silicon photodetector Newport 818-SL, which is a very sensitive device, was applied to measure the intensity output. A lock-in amplifier was also applied to remove the noise associated with the light source. The input and the output were also connected to a computer for checking accuracy. The setup was shown to produce stable results.

An inexpensive configuration developed by Cennamo, Monica and Zeni [20] successfully utilized POF in a temperature sensor. The fiber was coated with a layer of silicone. Under the effects of different temperatures, the RI of the silicone layer changes. Therefore, the propagation of light inside the fiber core is also altered. The sensor measured the temperature inside a water bath. A halogen lamp was used as the source, and the output was read by the VIS-NIR spectrometer. The intensities over a range of wavelengths were registered by the spectrometer at different thermal conditions. It was discovered that different sensitivities can be achieved at different wavelengths, with the best performance registered for light at 625 nm in a temperature range of 24-46°C. The authors suggested that the sensor can be used to monitor hyperthermia in cancer treatment.

The possibilities of using intensity modulation principle were further explored in the paper by Angelini et al. [21], where a POF sensor was used to detect hydrogen-sulfide (H_2S) gas. The proposed technique is cheap and also meets the demands of fire safety. In order for the gas to affect the mechanical composition of the fiber, the used fiber was covered with silver. The chemical reaction between H2S and silver results in the decline of the fiber’s propagating qualities. This degradation was observed through the diminished output,

allowing to make conclusions about the presence of the gas. It was advised by the researcher to remove a thin fluorinated layer on top of the fiber core by chemical etching before conducting experiments to make the device more sensitive. It was also determined that wavelength does not influence the quality of performance in this particular experiment, since similar results were obtained for 3 LEDs of different colors. A spectrometer manufactured by Avantes was used to detect the output. The drawback of the method was that other gases interfered with the detection procedure. The possible solution is to find a way to properly isolate the silver cladding. The proposed mechanism can be used to monitor the conditions of silver artifacts in museums.

2.2.1 POF-based sensor for detecting breathing rate

The sensing applications used for measuring breathing are discussed in the next paragraphs with the focus on configurations that utilize POF.

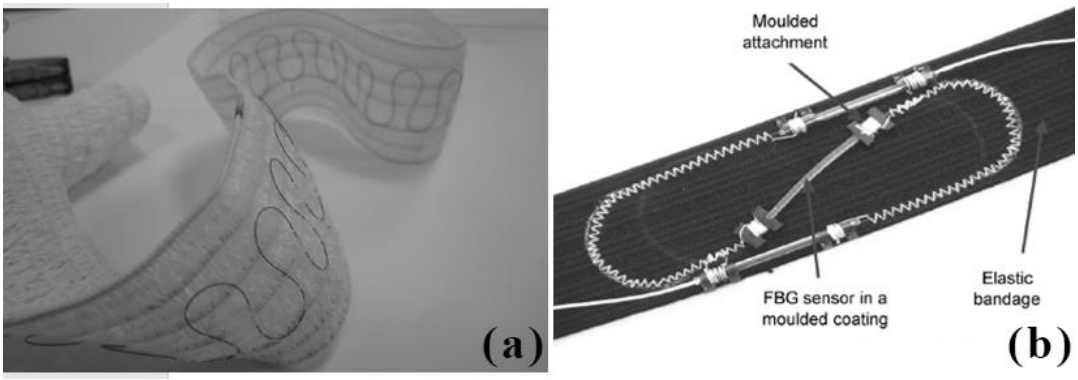

Figure 2.7: a) Macrobending POF-based sensor for measuring breathing; b) FBG sensor for measuring breathing [22]

The work by Witt et al. [22] explored the possibility of measuring respiration rate using a configuration based on optical fibers, which was comprised of two independent setups. The first one was a macrobending POF-based sensor utilizing intensity modulation, and the second was based on FBG. However, silica FBG was used, since FBG based on POF is not commercially

available. The authors stated that the proposed configuration can be utilized by patients at home. The immunity of the optical fiber transmissions to interferences from electro-magnetic fields is a quality that was considered very helpful by the authors, since the sensing setup was meant to be used simultaneously with magnetic resonance imaging (MRI). The macrobending sensor, shown in Figure 2.7a, was placed in abdominal area, while the FBG sensor, shown in Figure 2.7b, was placed in thoracic area. Both of the sensors were embedded in elastic belts. Superluminescent diodes (SLED) were used as the sources for the sensors. The fiber under the impact of macrobending become more sensitive to curvatures caused by breathing. The curvature of POF mirrored the deformations experienced by the textile. Then, the changes in the received intensity were monitored by a photodiode. When respiratory movements caused deformations in the fiber of the FBG sensor, certain wavelengths were reflected instead of being transmitted. The resulting spectrum was observed by optical interrogator Micron Optics sm130; it was also noted by the authors that the cost of FBG interrogators start from 10000€. The results obtained by the sensors were converted to electrical signals and compared, showing a close resemblance to each other. While being highly accurate and not complicated in handling, that setup required the use of sizeable and costly interrogator to read the output from the FBG sensor.

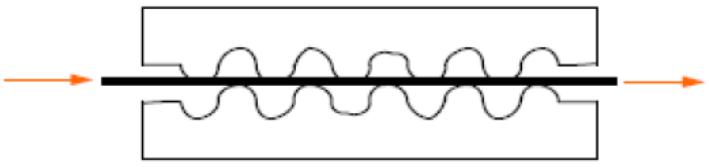

Figure 2.8: Fiber placed between two microbenders [23]

Chen et al. [23] developed a POF-based microbending sensor to measure breathing rate. Intensity modulation was used. The fiber was aligned between two microbenders. The setup, shown in Figure 2.8, was embedded into a cushion

for spine. A transceiver was used to supply light of 660 nm as the input and to read the output. It was connected to a computer for further processing. Then, the body vibrations occurring during breathing caused the change in the transmitted light according to the intensity modulation method. The information on the periodicity of the breathing was extracted from the resulting waveform using Fast Fourier Transform (FFT). Initially, the accuracy was checked by generating an input function and then comparing its period with the period of the output. The accuracy of 0.2 Hz was achieved. Then, the configuration was used to measure actual breathing. The respiration rate indicated by the sensing setup matched the manually counted rate.

The work by Vallan, Carullo and Casalicchio [24] explored in greater details how POF can be used to observe rate of breathing in medical conditions. The advantage offered by POF is that it can be used in conjunction with MRI while not being affected by its electric fields. The principle of intensity modulation was applied again. An LED at 650 nm was applied as the input, and an interrogation system was reading the output. A band-pass filter was added to remove frequency components beyond the range of 0.1-10 Hz. The fiber itself was attached to the chest of a patient. As a result, breathing was causing the cable to bend. However, POF was not very sensitive to mechanical bending, so additional measures were applied to make it more pliable. It was achieved by removing the exterior cladding, thus making the fiber's surface more rough. The procedure was accomplished through plasma etching. The fiber was permanently bent to soften it using thermal manipulations. It was recommended to attach the fiber to the lower part of the chest, because the significant level of curvature change that was caused by breathing happens there.

2.2.2 Sensors implemented by multiplexing POF

The papers in this subsection explored the possibility of multiplexing several POFs.

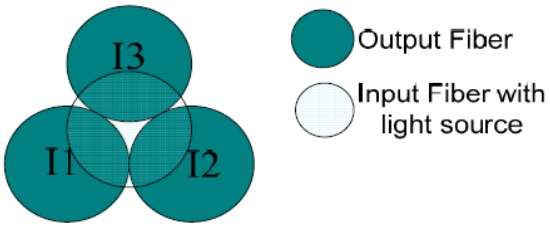

Figure 2.9. Multiplexed fibers for measuring back bending [1]

In the work by Kam et al. [1], bending of lower back was monitored by multiplexing 3 fibers. They were used to read the output and were coupled to a single fiber providing the input, as demonstrated by a scheme shown on Figure 2.9. The change in the curvature was causing the alteration of the input fiber position. As a result, the amount of light coupled into each of the output fibers was changing. It allowed to track the curvature level. The achieved operating range for measuring back curvature was from -12° to 12°. Beyond that values, the saturation of the sensor was observed.

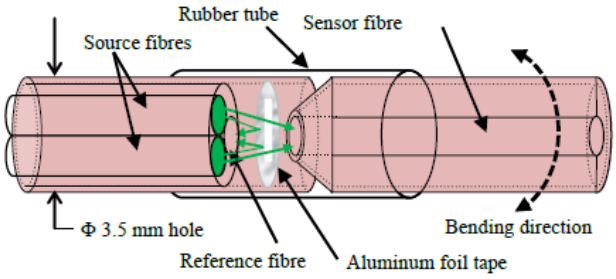

Figure 2.10: Setup for measuring spine bending [25]

Zawawi, O'Keeffe and Lewis [25] developed a technique to measure spine bending using POF. There is an increasing need in continuous monitoring of people with various spine conditions, and the existing sensors are not suitable to be used over long periods of time. The possible solution is to apply optical

sensors. The setup, which is shown in Figure 2.10, consisted of 2 parts. The first part contained 2 fibers that were connected to 2 identical green LEDs and a single fiber that was used as the reference. The model of the used LEDs is IF-E93, operating at 530 nm, and the reference was read by photodiode SFH-250 V. All of the fibers were placed parallel to each other, and a reflector made from aluminum foil was attached next to the fibers. It was used to reflect some portion of the input light back to the reference fiber. However, a window was cut in the reflector. As a result, there was a part of the input light that was not reflected and was able to propagate further. This light was coupled into a sensing fiber, which was placed in the second part of the setup. The place of coupling had to be positioned at the area where bending occurred. The bending section was equipped with the overlaying layer of rubber that kept the fibers connected. The sensor fiber was connected to a photodiode which was identical to the one that received the intensity from the reference fiber. At the output, the light from the sensor and the rest of the light from the reference were observed. Their ratio was then used to compensate for the interfering noise. The proposed configuration could measure spine bending in a range from 0° to 20° with the resolution equal to 2°. Such characteristics can provide a sufficient level of accuracy for the application in medicine.

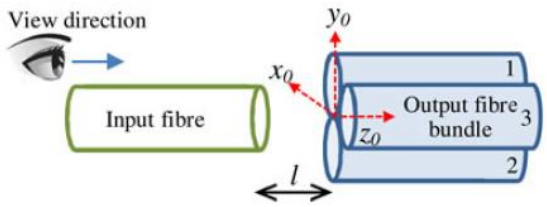

Figure 2.11: Setup based on automatic intensity compensation [26]

The same research team continued their work on measuring spine bending with POF [26]. It was reiterated that optical fiber sensors are immune to interference from electromagnetic fields. They also pose no danger for patients

in terms of the electrical shock possibility. In the experiment, 1 input fiber was coupled with 3 output fibers which were identical and, therefore, had the same loss in the light intensity. IF-E93 was used again as the light source, and 3 photodiodes of model SFH-250 V were receiving the light from the output fibers. When the sensing setup was bent, the position of the input fiber was changing relative to the output fibers. As a result, different amount of light was coupled into each of the receivers. The ratios of the outputs were then used for the accurate estimation of bending. The configuration can be observed in Figure 2.11. The operating range from -22° to 22° with the resolution of 0.1° was achieved. It was shown that the device was capable of differentiating between movements in lateral directions and flexion. It was also determined that the larger size of gap between the input and the outputs had a positive effect on the sensitivity. However, the range was decreased as a result. Then, it was suggested that the output needs to be collected very closely to the end of the fibers to avoid additional losses during transmission.

2.3 Sensors based on smartphones

The consideration of smartphones acting as the output detectors in sensors is provided next.

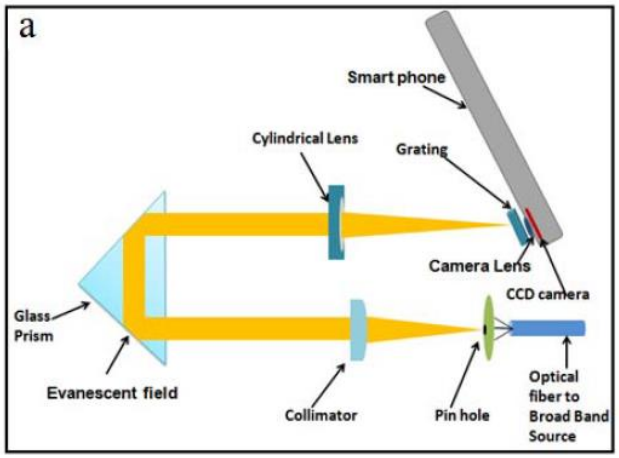

Figure 2.12: Smartphone acting as a spectrum analyzer [27]

Dutta, Choudhury and Nath [27] used a smartphone as a spectrum analyzer. Its advantages over other available spectrometers are low cost and portability, which is especially important for on-field procedures. The vast variety of communication tools inside smartphones makes it possible to quickly send the results of measurements to laboratories for further analysis. In the considered work, as shown in Figure 2.12, the smartphone was interfaced with a grating, a prism and cylindrical lens in order to disperse the incoming beam of light into its spectrum, which was observed at the camera. Then, the mixtures of water with the different concentrations of colored liquids were analyzed by the assembled system. The received images needed to be converted to grey scale. After that, the plot of the pixel distribution was created. It was demonstrated that it was possible to produce a reliable spectrum for each sample. The paper was the first work that considered this particular configuration for the spectrum measurements.

In the paper by Hossain et al. [28], the application of smartphones for the detection of pH in water was studied. The existing alternatives are complicated in exploitation. In addition, the proposed system is cheaper to implement. It also used the white LED of the camera as the light source. The chamber for the storage of the analyzed water samples and the prevention of interference from external illumination was assembled in 3D printer. It was attached to the smartphone camera. Water containing pH was illuminated by the source, resulting in the excitation of the studied sample. The corresponding alterations in the fluorescence intensity of the sample were traced by the camera. The researchers discovered that the proposed configuration can provide a stable performance under different conditions of the surrounding environment. The comparison with similar sensors showed that the smartphone system was capable of providing accurate results. The authors also suggested that the quality of the sensor can be increased by adding more lenses.

The paper by Gallegos et al. [29] also explored the ways to implement spectral analysis by smartphones, particularly in the area of biosensors. The approach considered by the authors was the measurement of wavelength shift in a photonic crystal. The coupler that aligns the camera with the crystal was made from aluminum, but it was mentioned that plastic can be used as alternative. The external source of light was used to excite the studied samples. The light that passed through the crystal was directed at the camera with the help of additional lenses. The grating was also set in front of the camera. The research group developed a mobile application to conduct the analysis of the received spectrum. As evidenced by the results, the system can offer a high sensitivity. The components used in the configuration are inexpensive, and the developed mechanism can serve as a viable alternative in cases when laboratories are not available.

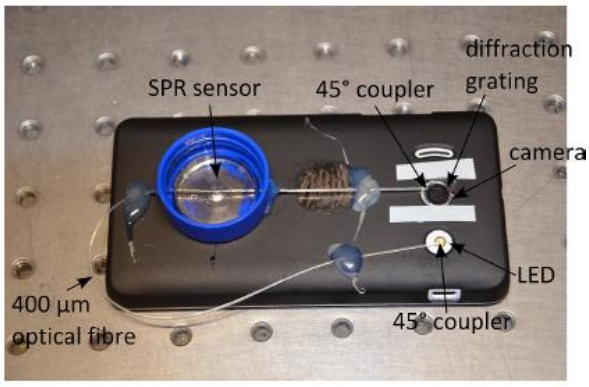

Figure 2.13: Setup based on smartphone and optical fiber to monitor the level of glycerol concentration [30]

The next paper by Bremer and Roth [30] was particularly helpful since it linked an optical fiber with smartphone. The purpose was to define the level of glycerol concentration in a liquid the sensor was immersed in. In the work, the fiber was coupled with the smartphone flashlight and the camera, which served as the light source and the detector, respectively. The theory behind the process is that the concentration affects the refractive index of the liquid, thus leading to

the alteration in the intensity of the propagating light. However, plastic cladded silica (PCS) instead of POF was used. The camera was equipped with a diffraction grating to ease the analysis of incoming wavelengths by looking at the line spectrums. During the preparation of the sensor, the fiber core was covered with a thin layer of silver to achieve the required sensitivity. The experimental setup can be seen in Figure 2.13. The system was tested for various concentrations. For each value, there was a noticeable shift in the received wavelength. It was inferred that the higher camera resolution can lead to the increase in sensitivity. The possible applications include medical and environmental monitoring.

2.4 Previous work

I previously participated in the development of an all-POF-smartphone sensor for the detection of hydrogen sulfide (H_2S) gas [31]. That configuration is a precursor to the currently considered implementation of the POF-based smartphone sensor for the measurement of breathing.

In that earlier work, the method of intensity modulation was used. The flashlight and the camera of a smartphone were used as the light source and the output detector, respectively. They were linked through the POF link. It was required to detect the presence of H_2S gas in the surrounding environment. The fiber coating was removed, and the core was covered with silver instead. The chemical reaction between H_2S and the silver layer caused degradation in the transmitting properties of the fiber link. It was shown that an increase in the level of H_2S caused a decrease in the amount of light observed by the camera.

2.5 Summary of the reviewed information

In section 2.1, 3 sensing approaches were considered. In FBG, the spectrum of the propagated light needs to be monitored. In order to observe the

wavelength shifts, the smartphone camera would have to be equipped with diffraction grating, while intensity modulation has no need for additional tools to monitor the propagated light. The surrounding medium of the breathing sensor is air, which means that low sensitivity would be achieved for the RI method, making intensity modulation the most suitable choice for the case at hand.

Then, the applications of POF-based sensors were reviewed. Intensity modulation was the most common approach. There are also breathing sensors which are based on POF. One of the considered examples applied FBG and utilized an expensive interrogator. However, other implementations of breathing sensor based on POF showed that simple LEDs and photodiodes can also be used to accurately monitor respiration. In addition, one of the method applied FFT to extract the frequency of breathing. The authors that applied plasma etching to POF noted that the lower area of chest leads to the highest sensitivity when measuring breathing. This observation is going to be used in the thesis.

After that, some works on multiplexing were considered. They acted as curvature sensors and also used the method of intensity modulation. However, each implementation was used to sense a single parameter. It was also noted that the receiving fiber needs to be placed as close as possible to a detection device to avoid losses of light.

Section 2.3 demonstrated some of the sensing applications that use smartphones. Two of them involved a mobile device acting as spectrum analyzer by equipping it with additional prisms. The authors of the papers on the first considered smartphone sensor suggested that the acquired data can be sent to a laboratory for further processing. A similar approach can be taken when detecting breathing rate, since the measurements can be quickly sent to doctors. The third work combined a smartphone with POF, showing that the sensitivity of the camera is sufficient for implementing intensity modulation.

Chapter 3 – Sensing methodology

The chapter presents the techniques implemented in the development of the sensor. Firstly, the method of intensity modulation is discussed. Then, the propagation of light inside POF in terms of geometry is analyzed. It is shown how the POF link is modified in order to track breathing activity. The link is going to consist of 2 parts, the transmitting and the receiving fibers. The displacement between them is modulated by breathing movements. It means that the implementation of a displacement sensor also needs to be considered, and the expected behavior of such sensor is shown in the first section of the chapter. After that, the collection of the measurements by the smartphone is discussed, followed by the overview of the couplers used to connect POF with the mobile device.

The 1st section of the chapter is mainly concerned with the programming tools used in the sensing procedure. The approach used in the simulation of the transmission between the 2 fibers in the POF link is demonstrated, as well as the extraction of breathing rate from the measurements using digital filtering. The simulated dependence of the transmission on the displacement between the fibers is also going to be used in the next chapter, where it will be compared with the actual measurements by the POF-based smartphone sensor. It needs to be done to ensure that the proposed configuration can be a reliable indicator of the intensity variation. The development of the smartphone application is also explained in the 2nd section.

The final section of the current chapter is devoted to multiplexing.

3.1 Working principle

3.1.1 POF parameters

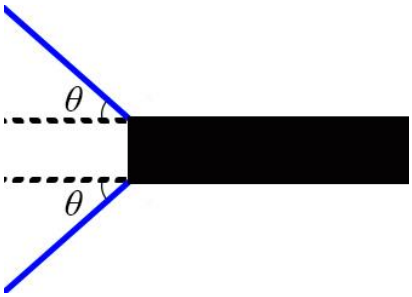

Figure 3.1: The critical angle of POF

First of all, we have to define the characteristics of POF that affect the transmission of light. PMMA, which is a material the fiber core is made of, has a refractive index equal to 1.49. POF is notable for its high numerical aperture, *NA*, which is usually equal to 0.47. This parameter describes a range of angles at which the fiber can receive or radiate light. In our case, the surrounding medium of the fiber is air, which means that the refractive index, *n*, is equal to 1. The direction of light rays incoming into the fiber core with the respect to the fiber core axis cannot be larger than some critical value, θ. The scheme is shown in Figure 3.1. The relationship between *NA*, *n* and θ is expressed through the following equation:

$$NA = n * sin\theta \tag{3.1}$$

From equation (3.1), the critical angle is approximately 28°. It means that it is not difficult to couple light into POF.

3.1.2 Intensity modulation

Intensity modulation is a method of analog transmission. It requires optical power to be transmitted through a fiber link. Optical power is produced by a source such as LED or laser placed at the transmitting end of the fiber. The amount of the received power is registered at the other end by direct detection,

which only requires photodetector to convert that output to a measurement with sensible units. As a result of changes in the surrounding medium or other external impacts, the fiber link experiences either deformations or other physical alterations. Since they affect the transmission properties of the link, the received power decreases. These changes in the output allow to make conclusions about the presence of elements affecting the performance. The process is illustrated in Figure 3.2.

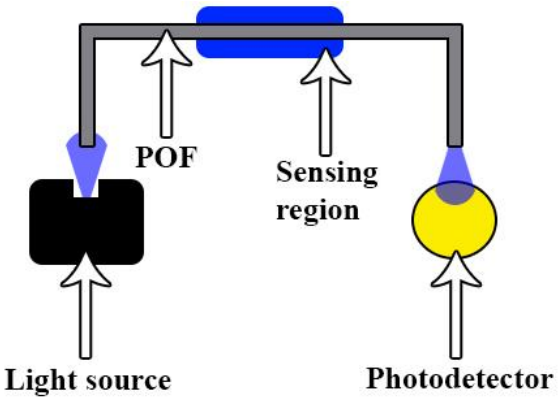

Figure 3.2: Schematic of intensity modulation

3.1.3 Modulating displacement

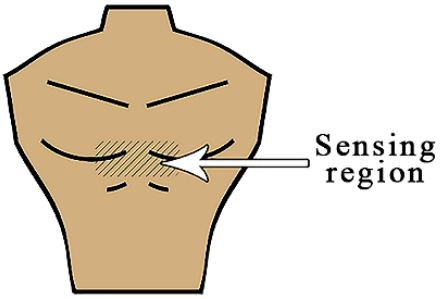

Figure 3.3: Placement of the sensor

Since breathing rate is measured, the alterations of the propagation properties inside the link need to be caused by respiratory movements. The lower area of chest was chosen for placing the link, as shown in Figure 3.3. According to Vallan et al. [21], that region experiences a change in curvature

that corresponds to the highest sensitivity during the measurements of respiration.

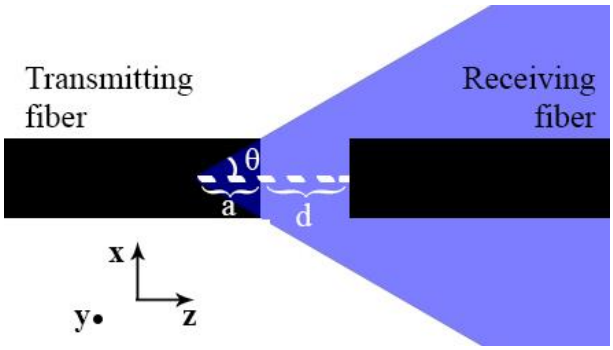

Figure 3.4: Transmission of light between two aligned fibers

The fiber link consists of 2 aligned POFs. The fibers are identical to each other. The radius of the fiber is denoted as r_f. The overall length of the POF link used in the measurements is 39 cm, but the system can operate with an arbitrary POF length up to several meters, limited only by the POF attenuation. The first fiber in the link couples the input light into the second one. The point of coupling needs to be attached to the sensing region. In the initial position, both the transmitting and the receiving fibers are horizontally aligned, as demonstrated in Figure 3.4. Each photon leaves the first fiber at some angle β that is not larger than the critical angle, θ. Until reaching the receiving fiber, the light travels over a distance equal to $z = a + d$, where a is the distance between the origin of the light ray and the surface of the transmitting fiber. It is defined as $a = \frac{r_f}{\tan\theta}$. Since the radius of the used fiber is 0.98 mm and the critical angle is equal to 28°, a is equal to 1.843 mm. d is the displacement between the fibers. In our case, the tested value of displacement is going to vary from 0 mm to 15 mm. The transmitted light intensity is defined by the following equation [11]:

$$I_t = \varepsilon \frac{P_{in}}{\pi r^2(z)} \tag{3.2}$$

Where P_{in} is the power from the light source, ε is the attenuation inside the fiber and *r(z)* is a radius of the light cone (colored blue in Figure 3.4) at point *z*. In this part, the ideal case with no attenuation is considered. The cone radius can be geometrically expressed as:

$$r(z) = z * \tan\theta = z * \frac{r_f}{a} \tag{3.3}$$

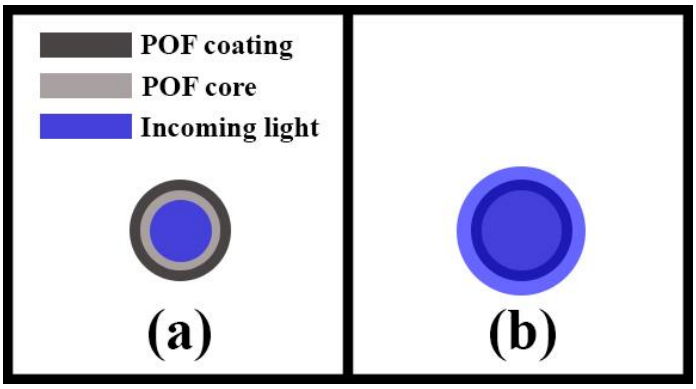

Figure 3.5: Illuminated area on the surface of the receiving fiber *a)* when the radius of the light cone is smaller than the radius of the receiving fiber; *b)* when the radius of the light cone is bigger than the radius of the receiving fiber

There are two cases of the illumination pattern. The first is when the radius of the illuminating cone, *r(z)* is smaller than the radius of the receiving fiber, r_f, i.e. when *d* is smaller than *a*, as can be seen in Figure 3.5a. The area illuminated on the surface of the receiving fiber is given by:

$$A(z) = r^2(z) * \pi \tag{3.4}$$

The power received is equal $P(z) = I_t * A(z)$, which means that expression (3.2) needs to be multiplied by expression (3.4), resulting in $P(z)=P_{in}$.

The second case is when *r(z)* is larger than r_f, i.e. when *d* is higher than *a*, which is shown in Figure 3.5b. The same conditions are observed in our case, since the critical angle of POF, which is 28°, will result in the illuminating cone completely covering the surface of the receiving fiber even at a displacement

equal to 15 mm. The illuminated area on the surface of the receiving fiber is defined as:

$$A(z) = r_f^2 * \pi \tag{3.5}$$

Similar to calculations in the first case, the received power is expressed as follows:

$$P(z) = P_{in} * \frac{r_f^2}{r^2(z)} \tag{3.6}$$

By substituting *r(z)* with (3.3) and *z* with $a + d$, (3.6) becomes:

$$P(z) = \frac{P_{in}}{(1+\frac{d}{a})^2} \tag{3.7}$$

By taking P_{in} as the normalized values of power, i.e. $P_{in}=1$, the overall dependence of the received power on the displacement can be drawn. The resulting curve is shown in Figure 3.6. The obtained relationship can be used to verify that the proposed sensor can function as a displacement sensor.

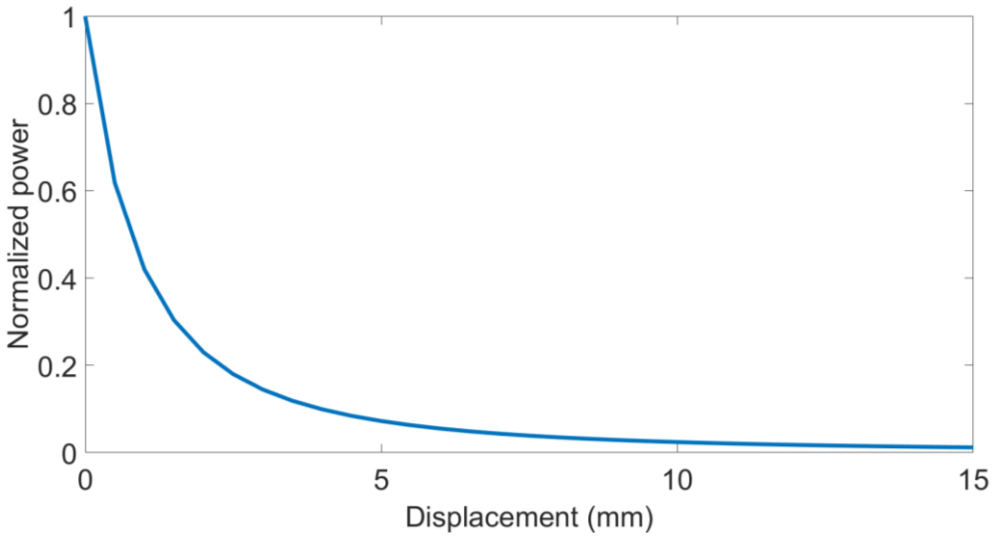

Figure 3.6: Dependence of the received power on the distance between fibers

In the implementation of the breathing sensor, the region of coupling needs to be placed on the sensitive region of chest. Before doing that, the

optimal value of displacement needs to be chosen from the 0-15 mm range, which is going be done with the actual measurements of displacement and corresponding intensities in the next chapter.

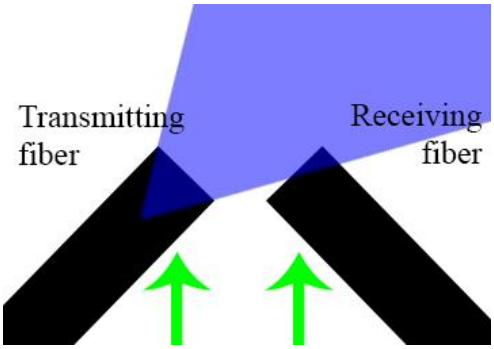

Figure 3.7: Transmission of light after angular displacement

As a result of breathing, the angular displacement between the cores of the fibers slightly change, and less light is coupled into the second part of the link in comparison to the initial state shown in Figure 3.4. This change in the position of the fibers is illustrated in Figure 3.7. It means that the periodicity of breathing over some specified time period can be determined by continuously monitoring the amount of light coupled into the receiver during that period.

3.1.4 Collection of information about intensities observed by smartphone

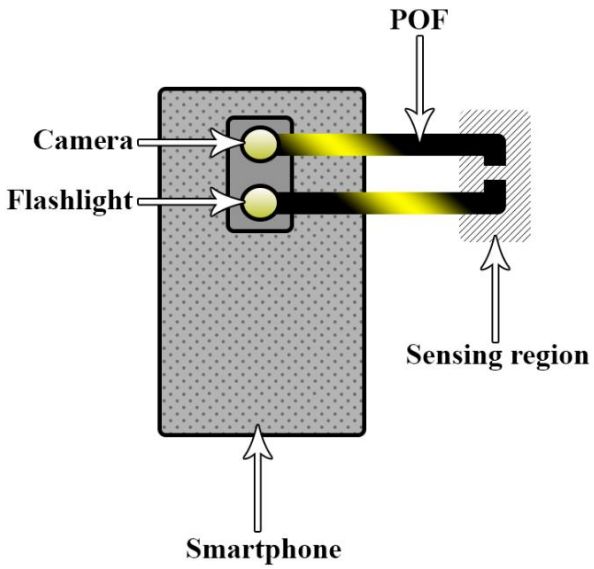

Figure 3.8: Intensity modulation based on smartphone

In our case, both input and output have to be provided by a hardware available in smartphones. The flashlight of a smartphone is used as the light source, and the smartphone camera reads the output, as shown by the schematic in Figure 3.8. However, contrary to photodetector which can directly obtain the power, the camera can only can be used to analyze the visual information about the signal. This is why first it has to be proved that the data registered by the camera can be a sufficient alternative to readings from photodetector. The proof is provided in the Results and Testing section.

The visual information is estimated by a sum of pixels on the image as seen by the camera (each frame has a size of *k*-by-*l* pixels):

$$Intensity = \sum_i^k \sum_j^l Pixel_{ij} \tag{3.8}$$

The example of the received image can be seen in Figure 3.9.

Figure 3.9: Image from the receiving fiber as observed by the camera

The actual implementation of the sensor includes the application specifically developed to accomplish the collection of such data by the smartphone architecture. However, commercial cameras usually automatically adjust their settings depending on the brightness of image. All of these features need to be accessed through the application code and deactivated. Otherwise, the results obtained by the camera will not be accurate. Moreover, settings that provide more stability in the measurements need to be identified. Since the

intensities are recorded with respect to time, the data is presented in the form of the waveform. Its periodicity is defined by applying FFT after filtering.

The fiber is going to be attached to the smartphone by a special connector. It will be manufactured using 3D-printer and can be seen in Figure 3.10. The connector was modelled in SolidWorks.

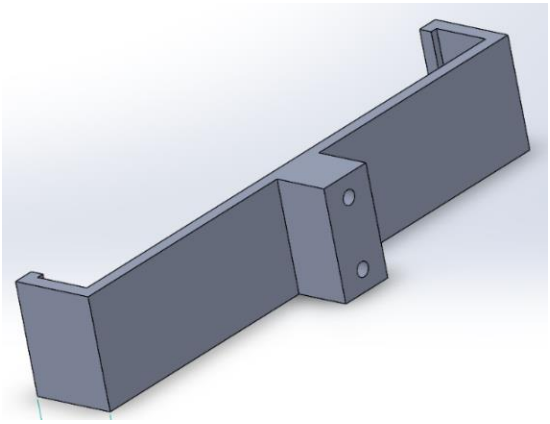

Figure 3.10: Connector for coupling fibers with smartphone

3.2 Programming setup

3.2.1 Simulation of the setup based on the displacement between fibers

The previously described geometrical approach does not fully match the realistic transmission of the light power. The transmitted intensity cannot be constant; Monte Carlo approach would be more accurate and useful for a simulation. The simulated results can be used to verify that the images captured by the camera are a reliable representation of the intensity variation. *M* photons are generated to represent the input. Each photon from the input light travels at some angles θ_x and θ_y with respect to *x* and *y* axes, which are perpendicular to line $z = a + d$ in Figure 3.4. The generated photon starts its propagation from the transmitting fiber if it satisfies the following condition with respect to the previously discussed critical angle [32]:

$$\theta_x^2 + \theta_y^2 < \theta^2 \tag{3.9}$$

For each photon, a random pair of angles (θ_x, θ_y) is generated. If the angles match the acceptable range, as specified by (3.9), the respective photon propagates further along direction *z*, as shown in Figure 3.4. The final *x* and *y* coordinates of the photon upon reaching the end of line *z* are defined as $z * \tan\theta_x$ and $z * \tan\theta_y$. The corresponding photon is accepted by the receiving fiber if these coordinates are within the area of the receiving surface, which was defined in (3.5). Then, the ratio of the accepted photons to the numerical value of *M* is calculated. The resulting dependence between the transmission and the displacement is shown in Figure 3.11. The implementation of the approach in Matlab is shown in Appendix A.1.

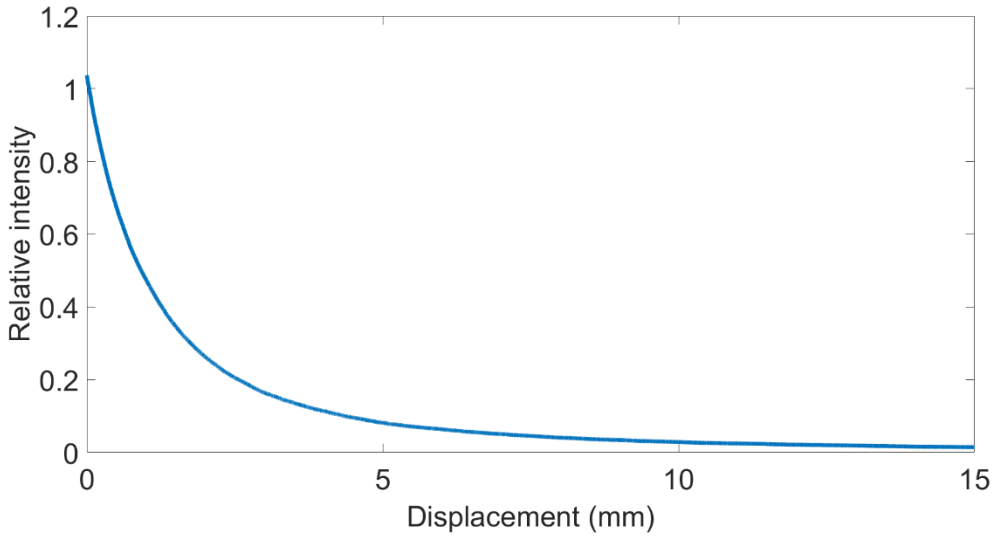

Figure 3.11: Simulated dependence of the received intensity on the displacement between fibers

The plot from Figure 3.11 is a more realistic representation of the relationship previously shown in Figure 3.6. Although the camera cannot directly detect power, which is the quantity that was analyzed so far in the chapter, it is expected that the intensity received by the smartphone will follow a curve similar to Figure 3.11.

3.2.2 Extraction of breathing rate

The changes in intensities associated with breathing activity result in measurements that have a sinusoidal form. Firstly, this signal requires filtering. It is implemented by a band-pass filter known as the Butterworth filter. It has a lower cutoff frequency equal to 0.24 Hz and a higher cutoff frequency equal to 1.06 Hz. The range is supposed to cover the common frequencies associated with breathing. The filter has to remove signals with frequencies close to 0. The response of the filter is shown in Figure 3.12.

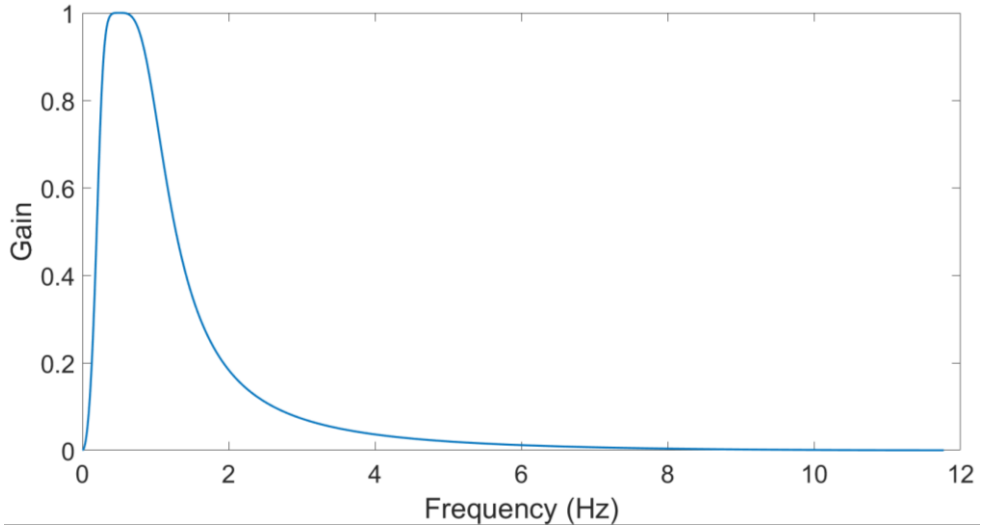

Figure 3.12: Frequency response of the applied Butterworth filter

After filtering, FFT is applied to obtain the information about the periods of the signals comprising the analyzed sinusoid. Due to the prominence of breathing movements, the highest frequency component is expected to indicate breathing rate.

3.2.3 Android application

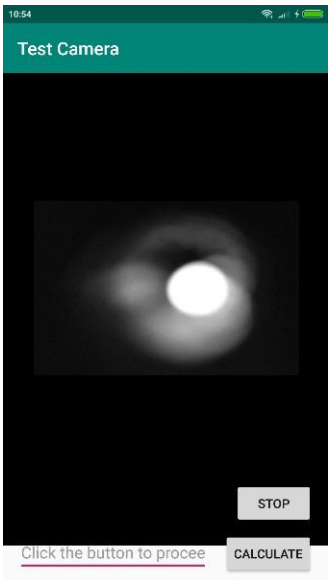

Figure 3.13: Interface of the application

The application for Android 7 was developed to set all of the required features and collect the sum of pixels. The programming language is Java. The compilation and debugging was done in Android Studio. The libraries of OpenCV were used to implement image processing. The visual interface is demonstrated in Figure 3.13.

Firstly, a class known as "*javaCameraView*" enables the use of native Android camera. Then, the code links the application with the layout from Figure 3.13. OpenCV of version 3.3.0 is initialized to make its libraries available to the application.

The "*javaCameraView*" class needs to be modified, since it sets camera parameters during the initialization of the application. The automatic adjustment of the exposition was removed by using a predefined function called "*setAutoExposureLock*." The default value of the exposition was set as 0. The function "*turnOnTheFlash*" was also added into "*javaCameraView*" by using a

predefined function called "*setFlashMode*." It was done to give the users control over activating the flashlight.

The matrix for storing the received image is introduced in the "*onCameraViewStarted*" function. The image is 8-bit and has 4 parameters. 3 of them are red, green and blue channels with possible values of intensity ranging from 0 to 255. The last parameter indicates transparency, having values between 0 and 1.

The "*onCameraFrame*" function is where the camera starts to receive the image and deliver it to the application. This function also activates the flashlight of the camera. The conversion of the image to grayscale is implemented, so that it has only one parameter for representing brightness. In order to save memory, the whole frames are not saved by the application. Only the pixel sums of each individual frames are going to be stored instead. The sum of the current frame seen on the camera is calculated by using a predefined function called "*sumElems*."

The sum is written as a string value to a text file in an internal directory of the smartphone memory by the "*writeToFile*" function. The function receives the value of the sum as the input and appends it to the file in the *txt* format.

The saving of the data by calling "*writeToFile*" is activated in the "*sendMessage*" function. It is linked to the button marked as "Start" in Figure 3.13. Once the button is pressed, the flashlight is activated through the "*turnOnTheFlash*" function and the app starts saving the pixel sums of the frames received by the camera in real time. The interval between saving the sums is 50 milliseconds. The process is interrupted once the "Stop" button is pressed. As a result, the sums from the frames received by the camera in the time period between pressing the buttons are stored in the text file. Since the sampling period is known (50 milliseconds), these values are ready to be plotted.

The resulting waveform is later analyzed to extract the periodicity of breathing. The whole code of the application can be found in Appendix A.2.

3.3 Multiplexing

For multiplexing, POF is tested as a curvature sensor. The same fibers are going to be used, but the link is not divided into two parts. There are 2 million propagating modes inside the standard POF for light rays to travel along. Light propagates in a zig-zag form, reflecting from the points between the core and the cladding. When bending is applied to the fiber, some of the rays begin to leak instead of being reflected. Due to changes in the curvature radius, the number of propagating modes decreases and less light is delivered. The multiplexing schematic can be seen in Figure 3.14.

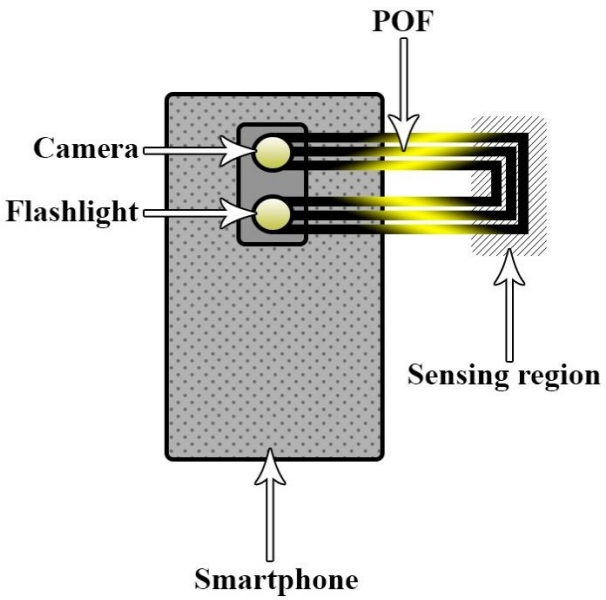

Figure 3.14: Intensity modulation using multiplexing

3 fibers will be multiplexed and tested. A new connector needs to be developed to accommodate them. Its model is shown in Figure 3.15.

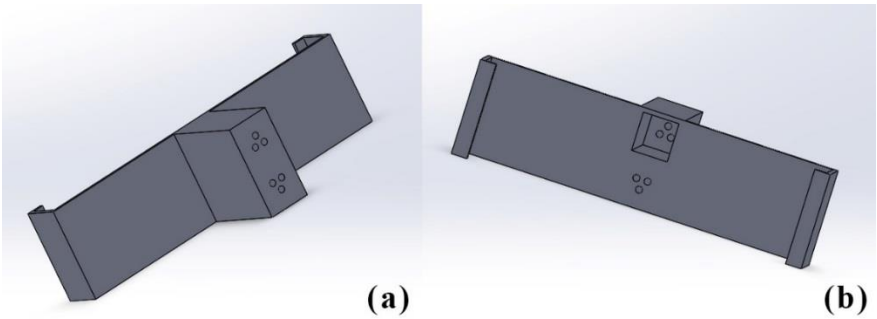

Figure 3.15: a) Front and b) back side of the connector for multiplexing

The upper 3 sockets are for coupling with the camera. Compared with the lower sockets, the upper ones are supposed to be located at a distance of 15 mm from the smartphone case, as demonstrated in Figure 3.15b. Otherwise, the fibers would be too close to the camera, and it would be impossible to differentiate between the received intensities. The lens of the camera is not wide enough to cover the images from 3 fibers at a distance shorter than 15 mm.

In the current work, it needs to be discovered whether each of the multiplexed fibers can act as an independent sensor.

Chapter 4 – Testing and Results

The chapter discusses the sensing process and the obtained measurements. Firstly, the custom-made connector is presented, and the optimal camera settings are determined. Then, the modulation of displacement as measured by the smartphone is shown. It needs to be done in order to verify that the proposed configuration can act as a displacement sensor and reliably indicate the changes in the intensity of the propagated light. Following this, the measurements of breathing activity are presented. The final section of the chapter considers the preliminary results obtained from multiplexing.

The fiber used for sensing is a standard perfluorinated POF made of PMMA, having 0.98/1 mm core/cladding diameter. The length of the POF link, as discussed previously, is 39 cm. The cost of POF is around 2.75$ per meter [33].

4.1 Designing connectors

The smartphone used in the experiments is Redmi Note 4 having dimensions 151 x 76 x 8.3 mm. The connectors were designed in SolidWorks to specifically fit that case. They were produced using polylatic acid (PLA) as a material in the 100%-fill printing. Their purpose is to firmly align the smartphone with the fibers and also to shield the camera from the ambient light of the surrounding environment. The cost of PLA is around 21$ per kilogram, but the connector is lighter than 50 grams. The connector for measuring the breathing rate is shown in Figure 4.1.

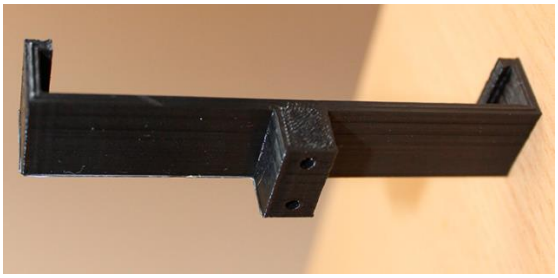

Figure 4.1: Connector for measuring breathing rate

The setup used in the experiments is in Figure 4.2. Sensing region needs to be attached to the lower part of the chest to start detection, as it was shown in Figure 3.3 from the previous chapter. The chosen area corresponds to high sensitivity.

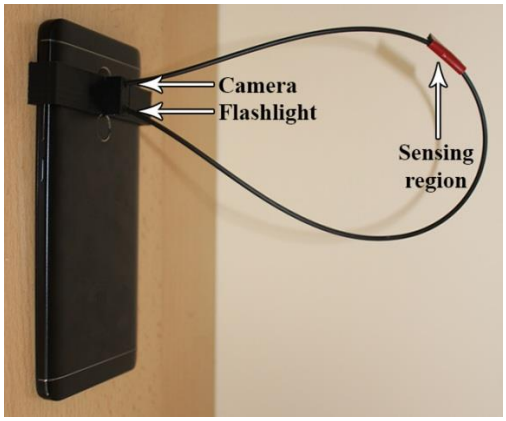

Figure 4.2: Sensing configuration used in the detection procedure

4.2 Calibrating camera

Since the measurement of the light intensity is required, the sensitivity of the camera to light is an important parameter. It is usually defined by a setting called ISO. Higher ISO indicates higher sensitivity, but it results in more noise on the received image. The right balance between sensitivity and noise needs to be found by choosing an appropriate ISO.

The calibration was implemented without applying any bending to the fiber. The position of the smartphone was fixed; POF was connected to transmit light. Then, the video was recorded for 5 minutes. The sum of pixels in a frame

was calculated after each 60 seconds beginning from the start of the video. After 5 minutes, there were 6 values of the sums. Then, the mean value and the corresponding standard deviation were calculated. The process was repeated for each ISO value. The results are summarized in Table 4.1.

Table 4.1: Intensities as recorded by the camera in the fixed position

ISO	0 min	1 min	2 min	3 min	4 min	5 min	σ	μ	σ/μ
100	1.365E+08	1.365E+08	1.366E+08	1.367E+08	1.370E+08	1.373E+08	3.353E+05	1.368E+08	0.245%
200	1.295E+08	1.297E+08	1.299E+08	1.300E+08	1.304E+08	1.305E+08	3.995E+05	1.300E+08	0.307%
400	1.303E+08	1.305E+08	1.306E+08	1.307E+08	1.310E+08	1.312E+08	3.376E+05	1.307E+08	0.258%
800	1.302E+08	1.303E+08	1.305E+08	1.306E+08	1.308E+08	1.310E+08	2.812E+05	1.306E+08	0.215%
1600	1.289E+08	1.291E+08	1.292E+08	1.294E+08	1.297E+08	1.298E+08	3.544E+05	1.294E+08	0.274%
3200	1.332E+08	1.336E+08	1.337E+08	1.339E+08	1.340E+08	1.340E+08	3.032E+05	1.337E+08	0.227%

(μ denotes the mean value and σ denotes the standard deviation)

The relative standard deviation is the ratio of σ to μ. From Table 4.1, the value of ISO equal to 800 provided more stability, as evidenced by the lowest relative standard deviation. Hence, it was chosen to be used in the experiment.

Then, it was required to discover whether the camera can provide an accurate measurement of the light intensity and also to find the value of a displacement between the transmitting and the receiving fibers resulting in higher sensitivity. The link consisting of the 2 fibers, discussed previously in the theoretical background, was established and connected to the smartphone. The dependence of the receiving intensity on the displacement between the fibers was tested. In the experiment, these 2 fibers were horizontally aligned. The displacement between them was changed from 0 mm to 15 mm with increments of 1 mm. The corresponding sum of pixels was registered for each displacement. The resulting relationship between the intensity and the displacement is shown in Figure 4.3. For the plot, the intensities were calculated relative to the first intensity, i.e., the sum of pixels on each image was divided by the sum of pixels on the first image.

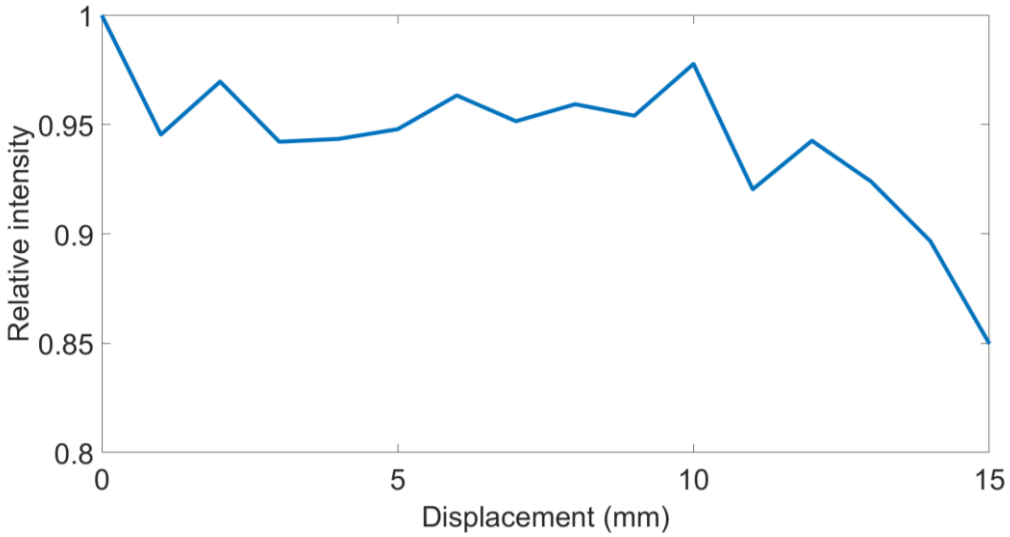

Figure 4.3: Dependence of intensity on the displacement between fibers (the camera exposition is set to automatic adjustment)

As it can be seen from Figure 4.3, the curve is disrupted by fluctuations. The intensity demonstrates an irregular behavior. The possible reason is the effect of the camera exposition, which automatically adapts to changes in brightness. Then, the experiment was repeated by locking the exposition. The fibers were placed on two linear micropositioners. Then, using micropositioners, the displacement between two POFs was changed from 0 mm to 16 mm with increments of 1 mm. The results can be seen in Figure 4.4.

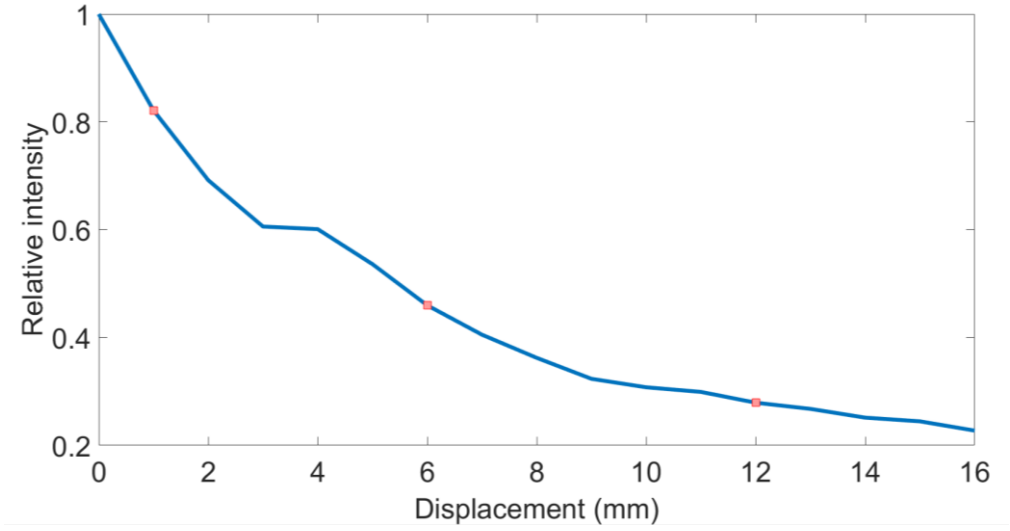

Figure 4.4: Dependence of intensity on the displacement between fibers

The results in Figure 4.4 are free of the disturbances seen in Figure 4.3 and in line with the expectations. An increase in the displacement leads to the drop in the intensity. At 6 mm, the intensity is approximately a half of the initial value. A plateau is reached at 12 mm. Although the sum of pixels does not necessarily correspond to the measurements of power, the overall shape of the curve in Figure 4.4 shows some resemblance to the relationship between the power and the displacement obtained during the simulation, shown in Figure 3.11, and a distinct intensity was registered for each displacement. It means that the integration of pixels can be used to track the changes in the light intensity.

As observed from the curve, the slope is steeper for lower values of displacement, especially for 1 mm. It indicates a higher sensitivity. Therefore, we set 1 mm as a default value for the gap between the fibers. It is the working point of the sensor, acting as a reference state. It indicates a position when no strain applied to the fiber.

The examples of images received by the camera at the 0 mm and 16 mm displacements during the experiment are demonstrated in Figure 4.5.

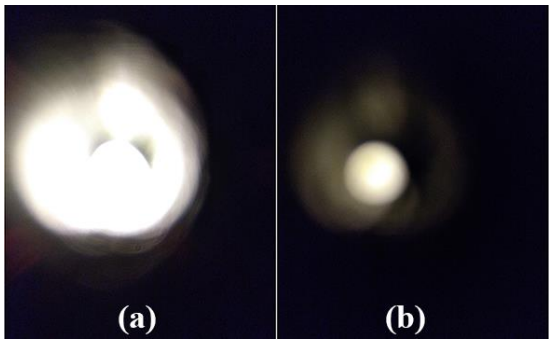

Figure 4.5: Intensities observed by the camera at the displacement values equal to *a)* 0 mm and *b)* 16 mm

4.3 Measuring breathing rate

The testing was done using third party application OpenCamera, since it allows more freedom in setting various camera features in comparison with

native Android programs. With all of the camera parameters specified, such as ISO=800 and no adjustment of the exposition, discernible pattern should be present in the waveform. The sensing region was attached to the chest with an adhesive tape. The measurements of breathing activity were taken for a period of 30 seconds and repeated 5 times. The resulting video was converted to a series of frames. Then, the images were processed in Matlab. Quiet breathing was monitored. The codes are in Appendix B.2. For the plots, the intensities in each period of measurements were calculated relative to the first intensity.

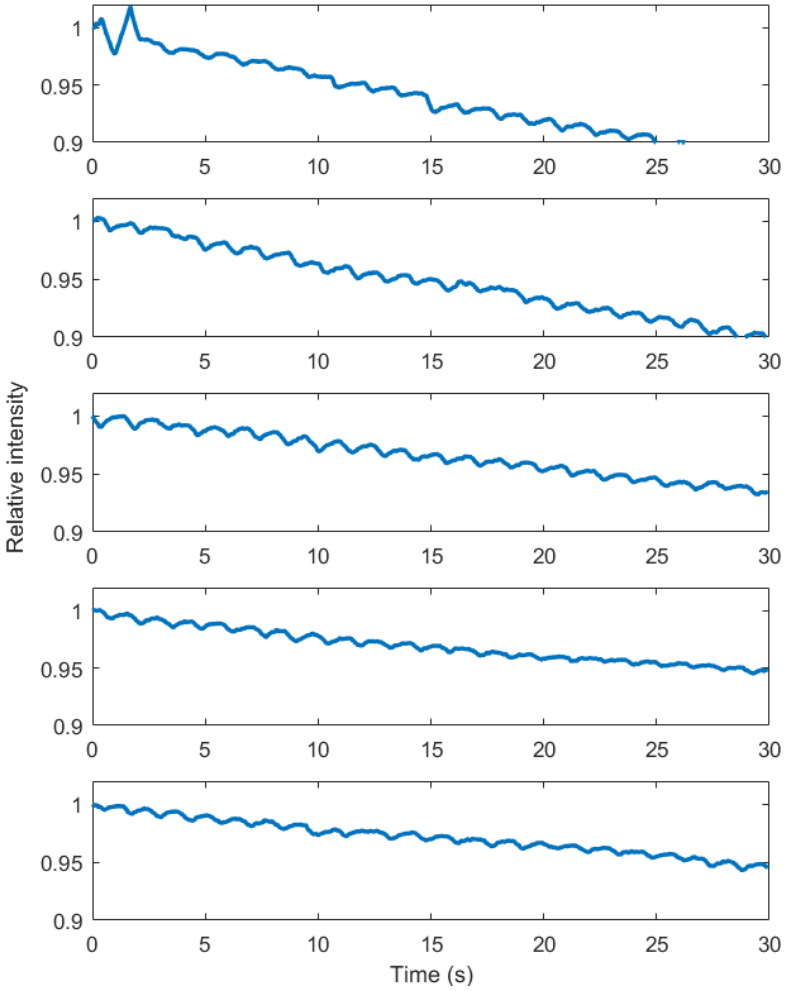

Figure 4.6: Breathing intensity as detected by the configuration at the 3 mm displacement

For example, the curve at 3 mm, as indicated by Figure 4.4, also has high sensitivity. We can additionally check that the 1 mm displacement results in

more stable measurements. The measurements of breathing activity registered with the 3 mm displacement are shown in Figure 4.6. Then, the same set of measurements was done for the 1 mm gap. It is shown in Figure 4.7. As expected, the higher stability is observed for the smaller displacement of 1 mm. The measurements from Figure 4.7 do not have strong downward trends which are present in Figure 4.6 and indicate unstable performance. The reason Figure 4.6 is free of such disturbances is that less stray light is coupled into the receiving fiber at the 1 mm displacement. Hence, 1 mm is indeed a more suitable choice. From this point, Figure 4.7 is considered.

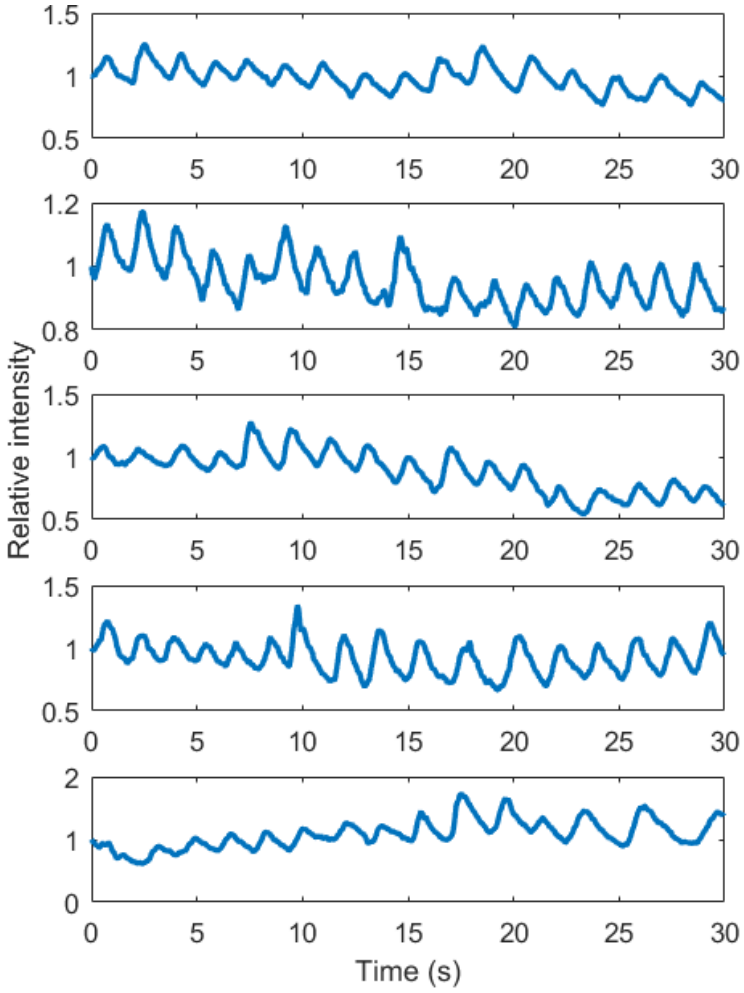

Figure 4.7: Breathing intensity as detected by the configuration at the 1 mm displacement

As expected, periodical signals are observed in Figure 4.7. However, noise of low frequency, which is similar to a DC signal, distorts the waveforms. Environmental light can cause such perturbations in the received signals. In addition, some of the signals have either upward or downward trend in intensity changes. Such behavior of the curves can be attributed to the previously discussed deviations occurring during the recording. In order to clear the waveforms, the previously discussed digital filtering was applied, resulting in the patterns shown in Figure 4.8. The signals are less affected by low and high frequency noises and correspond to the expected breathing patterns. The extraction of respiration frequency can now be implemented by analyzing the signals in frequency domain. For that purpose, FFT was applied.

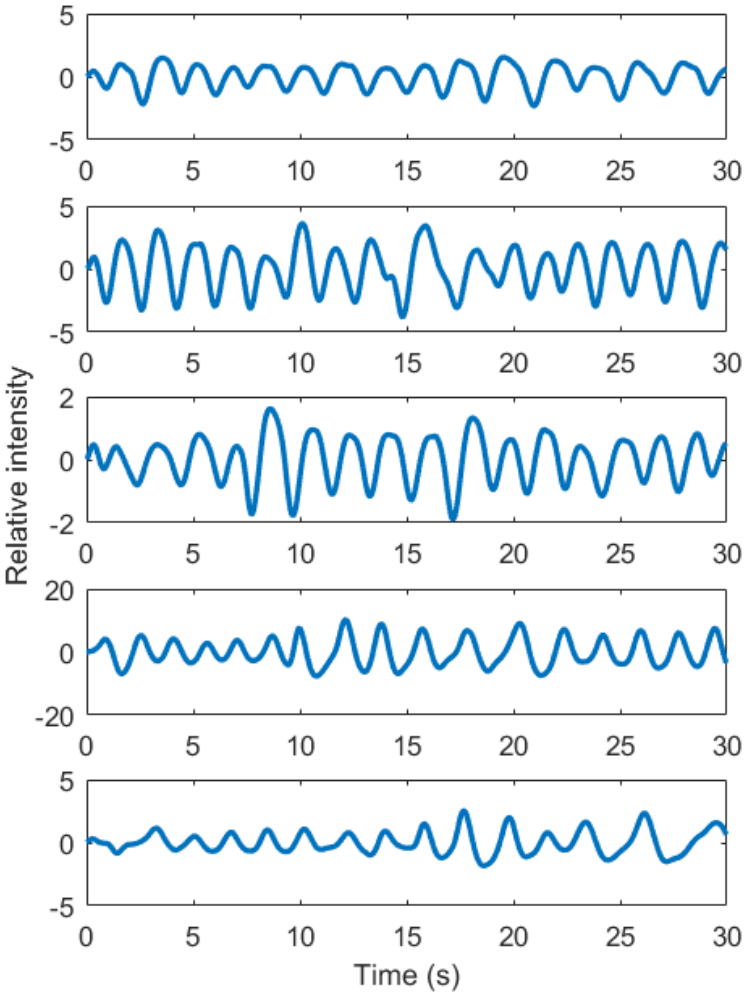

Figure 4.8: Breathing intensity after filtering

The spectral densities as a result of FFT are shown in Figure 4.9. The highest frequency component is observed at around 0.5 Hz, which corresponds to the average rate of breathing. Stronger fluctuations are seen in the spectral patterns of the 2nd and 4th experiments, since breathing was more intense. In the rest of the experiments, the intensities are lower due to quieter breathing.

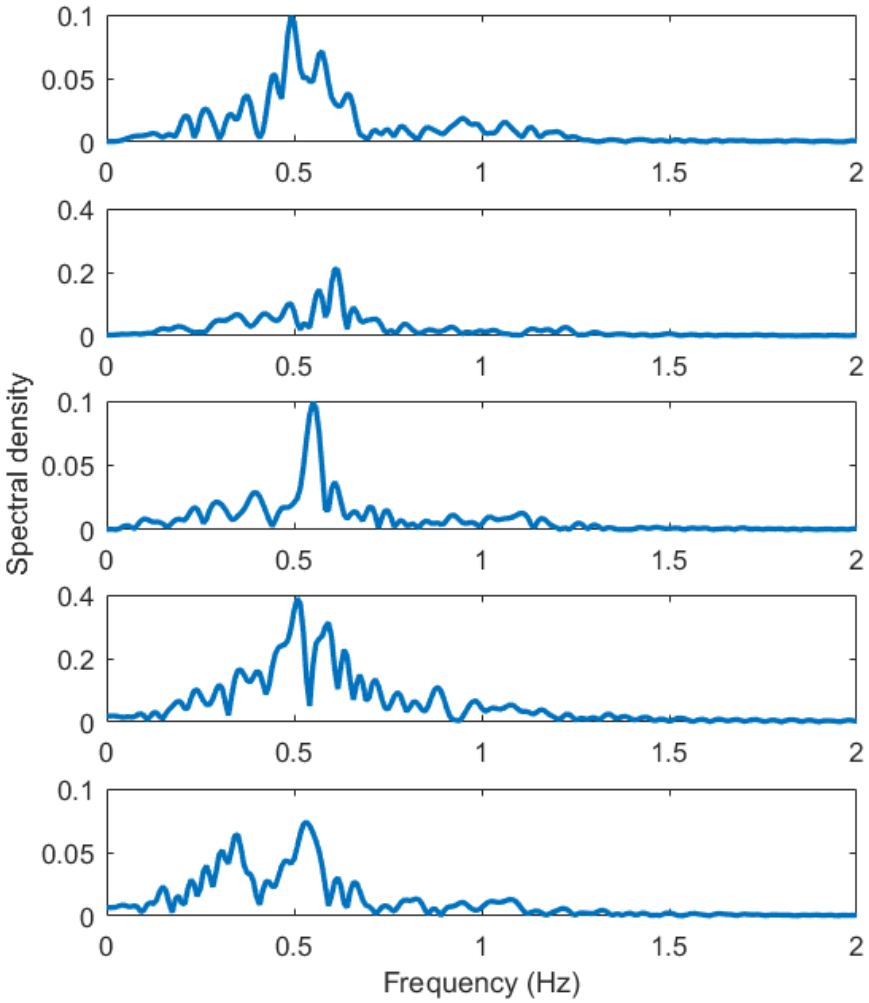

Figure 4.9: Breathing patterns in frequency domain

The accuracy of detecting breathing rate was measured by comparing the developed POF-based sensor with an accelerometer embedded in a different smartphone. The device detects the changes in acceleration of the smartphone along 3 axes in 3-dimensional space. Asus Zenfone 2 was utilized for that purpose. Its accelerometer has a recording frequency of 100 fps. It was placed

on the chest, so that the expansions during breathing change the position of the smartphone according to its *y* axis, as well as its acceleration in this direction. At the same time, the measurements were being made with the developed POF sensor. The setup is shown in Figure 4.10.

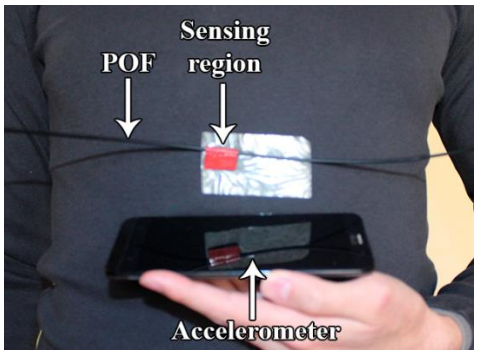

Figure 4.10: Placement of accelerometer

The filtering process discussed earlier was applied to the measurements made simultaneously by the POF sensor and the accelerometer taken as a reference. The resulting spectral densities are demonstrated in Figure 4.11. They both follow a similar shape. The frequency of 0.436 Hz was recorded by the developed POF-based sensor. The value obtained from the accelerometer is 0.447 Hz. The frequency measured by the proposed configuration differs only by 2.54% from the reference.

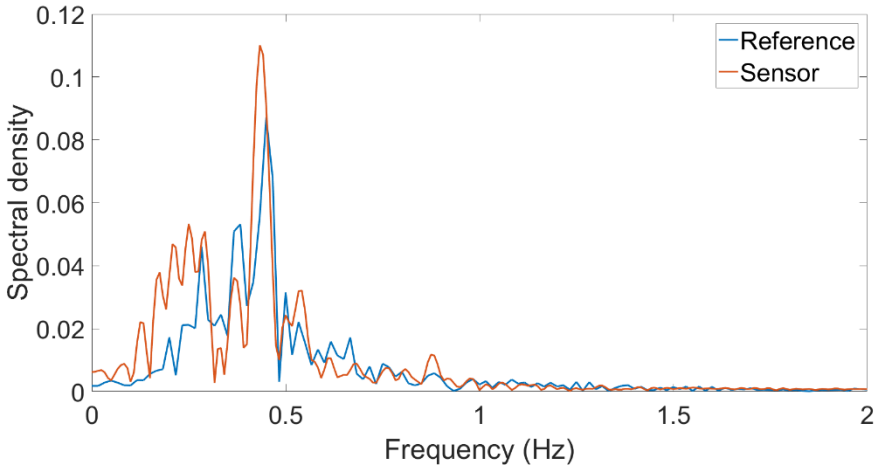

Figure 4.11: Comparison between the measurements taken simultaneously by the proposed sensor and the reference signal obtained by accelerometer

The differences in the measurements can be explained by uncertainties in the acquisition rates of the devices; the measurements by the POF sensor were taken at 17 fps. In addition, the performance in the case of POF is dependent on strain, while the accelerometer measures a position in space. This is why respiratory movements can result in slight variations across frequency responses.

4.4 Measurements by the Android application

The experiment was repeated using the developed Android application. The setup was the same, and the accelerometer was used at the same time as the sensor. For 30 seconds, the pixel sums of the images received by the camera during breathing were written into the text file inside the smartphone memory. It means that all of the data required for the extraction is located in a single file. There is no need to convert the video to a series of images and consume the memory of the smartphone, as it was done in the previous part. Quiet breathing was monitored.

Then, the file was imported to Matlab. Again, the information from the text file was digitally processed by the Butterworth filter to remove some interfering harmonics. Then, FFT was applied to obtain frequency components. Frequency of breathing should be the prevalent component.

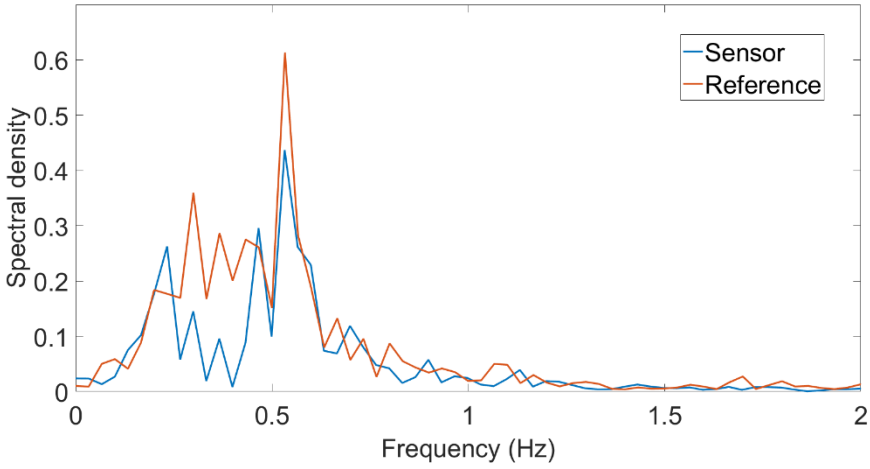

Figure 4.12: Measurements done by the application

The measurements taken with the application are shown in Figure 4.12. The peak frequency, which is breathing rate, can be easily extracted. The peak frequency as obtained by the developed sensor is the same as that of the accelerometer. In addition, the overall shapes of the spectrums are similar. The discrepancies can be attributed to different sampling rates. The sampling period of the developed application is 50 ms.

4.5 Multiplexing

3 fibers were connected to the smartphone camera for testing. Each was 21.3 cm long. The camera settings used for breathing were maintained. For these measurements, third party application OpenCamera was used again. We need to check whether each of the fibers can act as an independent sensor. Contrary to the case of measuring breathing, the displacement is not modulated. The fiber cores are tested as curvature sensors. For the first experiment, one of the fibers was slightly bent while the remaining two were in the state of rest. It was repeated for each of the fibers. The example of the received image is shown in Figure 4.13.

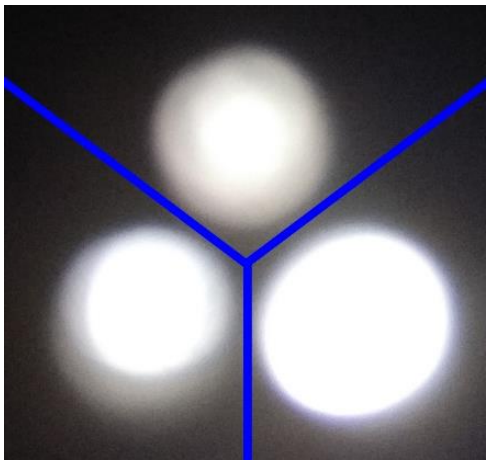

Figure 4.13: Image received from 3 multiplexed fibers

The image can be separated into 3 regions. For each region, the intensity was calculated as the sum of pixels, as it was done previously. It was expected

that only the bent fiber would experience a loss in the intensity and the remaining fibers, which were at rest, would experience no loss. The results are presented in Table 4.2. Instead of pixel sums, the relative losses in the received intensities with respect to a default state are shown. The default state is when no bending is applied to all of the fibers. The actual sums of pixels which were recorded in the measurements can be found in Appendix D.

Table 4.2: Measurements for 3 multiplexed fibers

Bent fiber	Relative losses in the intensity with respect to the default state		
	1st fiber	2nd fiber	3rd fiber
1st fiber is bent	10.84%	0.85%	1.61%
2nd fiber is bent	7.03%	5.87%	5.08%
3rd fiber is bent	1.62%	1.84%	5.28%

The significant drop in the transmitting performance can be clearly noticed only in the case when the 1st fiber was bent. The intensity was reduced by almost 11% in the 1st fiber, while the intensities in the remaining fibers experienced almost no change. When the 3rd fiber was bent, it lost 5.28% of the intensity, which was small in comparison with the 1st and the 2nd fibers that were at rest and experienced 1.62% and 1.84% losses, respectively. When the 2nd fiber was bent, its intensity was also reduced by almost 6%, but 7% were lost in the 1st fiber, which was in the state of rest. It was expected that bending one of the fibers would not affect the intensities in the unbent fibers. Such irregularities mean that POF cannot be reliably used as a curvature sensor without some modifications.

In addition, as it can be seen from Figure 4.13, unequal amount of light was coupled into each of the fibers, indicating possible inaccuracies during the manufacturing of the connector. They can be attributed to the precision level of Ultimaker extended 2+, which was used to print the connector.

POF is not sensitive enough to reliably measure curvature. This is why its propagating properties need to be weakened. It was done by cutting a very thin region on the surface of the fiber. The length of the region is approximately 1 cm. Due to the cuts, the integrity of the fiber core was disrupted. As a result, more light was expected to leak from the bent POF. The changes to the schematic shown previously in Figure 3.14 are reflected in Figure 4.14.

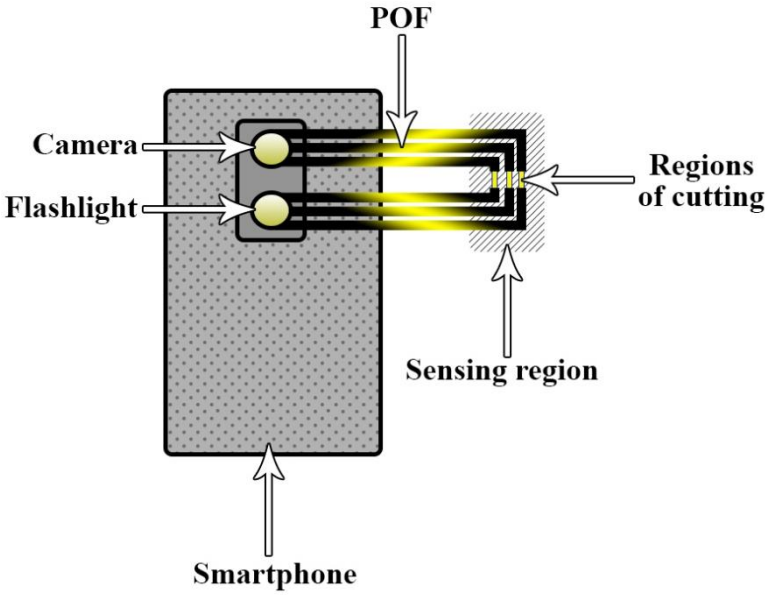

Figure 4.14: Intensity modulation using 3 multiplexed fibers with cut regions

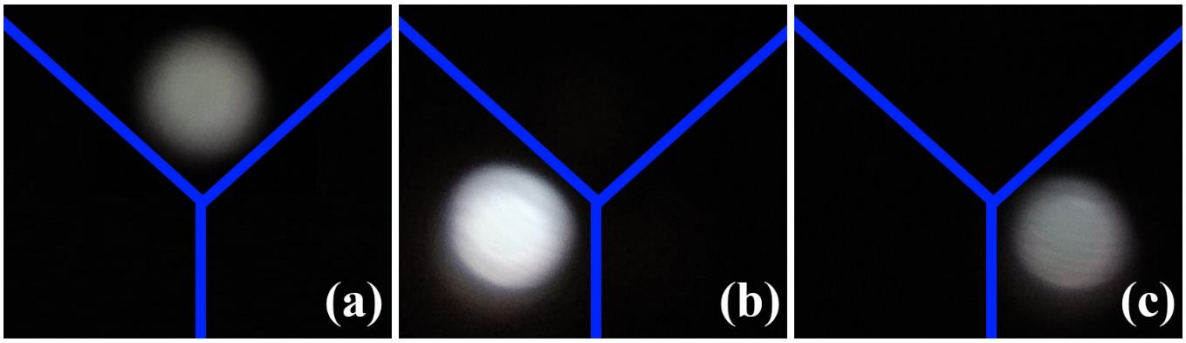

Figure 4.15: Images received by the camera when a) only the 1st fiber is connected; b) only the 2nd fiber is connected; c) only the 3rd fiber is connected

At first, the fibers were coupled to the smartphone through the connector one by one. It is represented by Figure 4.15. It was done to see how they behave

separately. A bending of 10° was applied in each case. The results are shown in Table 4.3.

Table 4.3: Intensities when 3 cut fibers are connected one by one

Considered fiber	State of fiber	Sum of pixels	Relative change between states
1st fiber	At rest	9.85E+06	51.62%
	Bent	4.77E+06	
2nd fiber	At rest	2.42E+07	17.04%
	Bent	2.01E+07	
3rd fiber	At rest	1.07E+07	36.59%
	Bent	6.80E+06	

It is clear that significant drops in the received intensities are observed. It means that weakened POF can indeed be used as a curvature sensor. Then, all of the fibers were connected. Deformations by 10° and 20° were applied to the 1st fiber while keeping the remaining two at rest. It was repeated for the 2nd and 3rd fibers as well. The results are in Table 4.4. As in the case of Table 4.2, relative losses are reported. The negative values indicate intensity gains. The sums of pixels used in the calculations can be found in Appendix D.

Table 4.4: Measurements for multiplexing 3 cut fibers

Bending angle	Bent fiber	Relative losses in the intensity with respect to the default state		
		1st fiber	2nd fiber	3rd fiber
10°	1st fiber is bent	12.95%	-2.93%	8.76%
	2nd fiber is bent	1.60%	-4.33%	6.82%
	3rd fiber is bent	41.16%	12.32%	37.18%
20°	1st fiber is bent	41.05%	-7.63%	-1.36%
	2nd fiber is bent	-2.83%	27.79%	5.25%
	3rd fiber is bent	9.01%	0.47%	4.31%

In the case of bending by 10°, the results are irregular. When bending the 1st fiber, the intensity dropped by approximately 13%, which was not significantly higher than a loss of 8.76% in the 3rd fiber. The bending of the 2nd

fiber caused an increase of 4.33% in its respective intensity. At the same time, the 3rd fiber lost 6.82%. A 37.18% loss in the 3rd fiber was observed when it was bent by 10°. In each of the cases, the expected behavior was not observed. The bending of the fiber is supposed to cause a change in the respective intensitiy that is easily distinguishable from the transmissions in the unbent fibers.

However, the deformation of the 1st fiber by 20° caused a drop of 41% in the corresponding intensity, while the received intensities in the 2nd and the 3rd fibers were increased by approximately 8% and 1%, respectively. The 2nd fiber lost almost 28% as a result of being bent by 20°, while the 1st and 3rd fiber experienced an increase of 2.83% and a loss of 5.25%, respectively. In these two aforementioned cases, the behavior is closer to the expected one, since the losses of the bent fibers were considerably higher than the intensity changes observed in the unbent fibers. However, that was not the case with the 3rd fiber, where bending by 20° did not significantly change the intensity of this POF.

Moreover, since equal level of bending was applied to each fiber, it was expected that each one of them would experience similar losses, which was not the case. The explanation for such irregularities is that the fibers are not identical as a result of cutting. Therefore, different amount of light was coupled into each of the receiving sockets. It is also possible that camera settings that result in high sensitivity of one fiber are not suitable for the others. While the camera detects changes in one of the fibers, it may not be as sensitive in the cases of the remaining fibers due to being saturated by the light it receives from them.

After that, the measurements were repeated, but only 2 fibers were multiplexed due to the irregular performance in the third socket. The bending of 20° was applied, since 10° was not causing a level of change that was enough to distinguish which fiber was bent. Firstly, the fibers were tested independently. The results are shown in Table 4.5.

Table 4.5: Intensities when 2 cut fibers are connected one by one

Considered fiber	State of fiber	Sum of pixels	Relative change between states
1st fiber	At rest	1.67E+06	59.63%
	Bent	6.72E+05	
2nd fiber	At rest	9.25E+05	33.88%
	Bent	6.12E+05	

From Table 4.5, the 1st fiber lost 60% of the intensity, and the 2nd fiber lost 34%. Then, the fibers were connected together. Each fiber experienced a 20° deformation in rotation. The results can be seen in Table 4.6. The relative losses are reported; the original pixel sums can be found in Appendix D.

Table 4.6: Measurements for multiplexing 2 cut fibers

Bent fiber	Relative losses in the intensity with respect to the default state	
	1st fiber	2nd fiber
1st fiber is bent	31.06%	5.61%
2nd fiber is bent	9.04%	20.10%

When the 1st fiber was bent, it lost 31% of the intensity, while the 2nd one experienced a loss of approximately 6%. When the 2nd fiber was bent, the corresponding intensity was reduced by 20%, while the 1st one lost 9%. Similar to the case of the bending by 20° in Table 4.4, the losses in the bent fibers were significantly higher than the losses in the fiber experiencing no deformations. However, ideally, the unbent fibers would not experience any intensity changes. It is possible that the present deviations result from the camera settings, since ISO can contribute to the noise level in the image. Another possible explanation is a crosstalk between the fibers. The cut regions of the fibers, as seen in Figure 4.14, were not covered by the fiber jacket. The light leaking from one of the fibers was possibly coupled into the others. Nevertheless, it was possible to monitor bending by 20°, since deformation of each of the two fibers resulted in the clearly distinguishable intensity change.

Chapter 5 – Conclusion

5.1 Summary

The sensor for the breathing intensity detection was designed using the smartphone architecture and POF. It was shown that the smartphone camera is sensitive enough to indicate the changes in the light intensity transmitted by POF and can be used as an alternative to photodetectors in the transmission scheme. The flashlight of the smartphone was used as the light source.

The transmission link was established by the pair of POFs. They were horizontally aligned, but a small gap was set between the fibers. Then, these fibers were attached to chest in a way that causes respiratory movements to slightly change this displacement.

The camera was also calibrated to have suitable features for monitoring the changes in the light intensity associated with breathing activity. As a result, the proposed configuration was shown to have a level of accuracy similar to the accelerometer which was also used to detect breathing rate.

The Android application was developed. It sets all of the required camera settings for monitoring breathing, and the obtained measurements are in agreement with the accelerometer as well. The application also provides the results in a form that allows easy processing.

Considering the sufficient results, the proposed configuration is a fitting tool for applications in telehealth due to being easy in use and compact. Another advantage is cost effectiveness, since POF and fabrication of connector are not expensive, and smartphones are already widespread among a vast number of people. As it was mentioned before, people diagnosed with COPD can benefit from measuring their breathing rates on a daily basis with the developed sensor;

if an increase in the intensity of respiration is registered, preventive measures need to be taken to avoid the exacerbation of the disease.

It was also shown that multiplexing can be implemented in the POF-based smartphone sensor. It was possible to monitor a bending of 20° by two multiplexed fibers.

5.2 Future work

A possible way to further improve the performance of the breathing sensor is to embed it into wearable textile. It will allow to completely shield the fiber from any stray light. Moreover, as a result of the textile flexibility, the fiber inside it can follow the changes in the chest shape during breathing more accurately, since more points on the surface of POF will be in direct contact with the sensing area. Textile also simplifies the placement of POF on the chest of the patients. It is more effective than attaching the fiber with adhesive tapes, and can provide higher level of comfort.

In addition, preliminary works on the implementation of multiplexing with the POF-based smartphone sensors were conducted, but the results can be improved. In order to proceed, equal amount of light should be coupled into each of the fibers when they are not bent. For this purpose, a new connector will be manufactured for multiplexing. Equal degradations of performance in the fibers could not be achieved by cutting. A possible solution is to weaken the propagating properties of POF by chemical reactions. The concentrations and amounts of chemical solvents are easier to evaluate and distribute equally between the fibers than mechanical deformations caused by cutting.

Bibliography/References

[1] W. Kam, K. O'Sullivan, W. S. Mohammed, and E. Lewis, "Low cost portable sensor for real-time monitoring of lower back bending," in *Proc. 25th Opt. Fiber Sensors Conf. (OFS)*, Jeju Island, Korea, April 2017, pp. 4.

[2] D. Z. Stupar, J. S. Bajić, L. M. Manojlović, M. P. Slankamenac, A. V. Joža, and M. B. Živanov, "Wearable Low-Cost System for Human Joint Movements Monitoring Based on Fiber-Optic Curvature Sensor," *IEEE Sensors J.*, vol. 12, no. 12, pp. 3424-3431, 2012.

[3] A. M. Yañez, D. Guerrero, R. Pérez de Alejo, F. Garcia-Rio, J. L. Alvarez-Sala, M. Calle-Rubio, R. M. de Molina, M. Valle Falcones, P. Ussetti, J. Sauleda, E. Z. García, J. M. Rodríguez-González-Moro, M. Franco Gay, M. Torrent, and A. Agustí, "Monitoring breathing rate at home allows early identification of COPD exacerbations," Chest, vol. 142, no. 6, pp. 1524-1529, 2012.

[4] S. Negi, R. K. Singh, and C. S. Anoop, "Development of a real-time breathing-rate monitor using difference operation method and adaptive windowing on dry-electrode ECG signal," in *Proc. 39th Annu. Int. Conf. IEEE Eng. Med. Biol. Soc. (EMBC)*, Jeju Island, Korea, July 2017, pp. 1529-1533.

[5] Elisa Spanò, Stefano Di Pascoli, and Giuseppe Iannaccone, "Low-Power Wearable ECG Monitoring System for Multiple-Patient Remote Monitoring," *IEEE Sensors J.*, vol. 16, no. 13, pp. 5452-5462, 2016.

[6] A. D. Jurik and A. C. Weaver, "Remote Medical Monitoring," *Comput.*, vol. 41, no. 4, pp. 96-99, 2008.

[7] D. Feng, J. Kim, M. Khadra, D. L. Hudson, and C. Roux, "Guest-Editorial Telehealth Systems and Applications," *IEEE J. Biomed. Health Informat.*, vol. 19, no. 1, p. 81, 2015.

[8] D. Zhanwei and Y. Yongjian, "Semi-automatic remote medicine monitoring system of mobile users," *China Commun.*, vol. 12, no. 11, pp. 1-9, 2015.

[9] Christopher G. Scully, Jinseok Lee, Joseph Meyer, Alexander M. Gorbach, Domhnull Granquist-Fraser, Yitzhak Mendelson, and Ki H. Chon, "Physiological Parameter Monitoring from Optical Recordings With a Mobile Phone," *IEEE Trans. Biomed. Eng*., vol. 59, no. 2, pp. 303-306, 2012.

[10] Daniël Lakens, "Using a Smartphone to Measure Heart Rate Changes during Relived Happiness and Anger," *IEEE Trans. Affect. Comput*., vol. 4, no. 2, pp. 238-241, 2013.

[11] A. Lopez-Aldaba, D. Lopez-Torres, C. Elosua, J.-L. Auguste, R. Jamier, P. Roy, F. J. Arregui, and M. Lopez-Amo, "Relative humidity multi-point optical sensors system based on Fast Fourier multiplexing technique," in *Proc. 25th Opt. Fiber Sensors Conf. (OFS)*, Jeju Island, Korea, April 2017, pp. 4.

[12] P. Polishuk, "Plastic optical fibers branch out," *IEEE Commun. Mag*., vol. 44, no. 9, pp. 140-148, 2006.

[13] L. Bilro, N. Alberto, J. L. Pinto, and R. Nogueira, "Optical Sensors Based on Plastic Fibers," *Sensors*, vol. 12, no. 9, pp. 12184-12207, 2012.

[14] J. B. Faria, "A Theoretical Analysis of the Bifurcated Fiber Bundle Displacement Sensor," *IEEE Trans. Instrum. Meas*., vol. 47, no. 3, pp. 742-747, 1998.

[15] H. Z. Yang, X. G. Qiao, D. Luo, K. S. Lim, W. Y. Chong, and S. W. Harun, "A review of recent developed and applications of plastic fiber optic displacement sensors," *Meas*., vol. 48, pp. 333-345, 2014.

[16] H. Cheng-Yua, Z. Yi-Fan, Z. Meng-Xi, L. L. M. Gordon, and L. Li-Qiang, "Application of FBG sensors for geotechnical health monitoring, a review of sensor design, implementation methods and packaging techniques," *Sensor and Actuators A*, vol. 244, pp. 184-197, 2016.

[17] L. Bilro, N. J. Alberto, L. M. S´a, J. d. L. Pinto, and R. Nogueira, "Analytical Analysis of Side-Polished Plastic Optical Fiber as Curvature and Refractive Index Sensor," *J. Lightw. Technol*., vol. 29, no. 6, pp. 864-870, 2011.

[18] H. Z. Yang, X. G. Qiao, K. S. Lim, S. W. Harun, W. Y. Chong, Md. R. Islam, and H. Ahmad, "Optical Fiber Sensing of Salinity and Liquid Level," *IEEE Photon. Technol. Lett.*, vol. 26, no. 17, pp. 1742-1745, 2014.

[19] Z. Harith, N. Irawati, H. A. Rafaie, M. Batumalay, S. W. Harun, R. M. Nor, and H. Ahmad, "Tapered Plastic Optical Fiber Coated With Al-Doped ZnO Nanostructures for Detecting Relative Humidity," *IEEE Sensors J.*, vol. 15, no. 2, pp. 845-849, 2015.

[20] N. Cennamo, A. D. Monica, L. Zeni, and P. Zuppella, "An optical temperature sensor based on silicone and plastic optical fibers for biomedical applications," in *Proc. IEEE Int. Instrum. Meas. Technol. Conf. (I2MTC)*, Torino, Italy, May 2017, pp. 5.

[21] E. Angelini, S. Grassini, A. Neri, M. Parvis, and G. Perrone, "Plastic Optic Fiber Sensor for Cumulative Measurements," in *Int. Instrum. Meas. Technol. Conf. (I2MTC)*, Singapore, May 2009, pp. 5.

[22] J. Witt, F. Narbonneau, M. Schukar, K. Krebber, J. D. Jonckheere, M. Jeanne, D. Kinet, B. Paquet, A. Depre, L. T. D'Angelo, T. Thiel, and R. Logier, "Medical Textiles With Embedded Fiber Optic Sensors for Monitoring of Respiratory Movement," *IEEE Sensors J.*, vol. 13, no. 1, pp. 246-254, 2012.

[23] Z. Chen, J. T. Teo, S. H. Ng, and X. Yang, "Plastic optical fiber microbend sensor used as breathing sensor," in *IEEE Sensors Proc.*, Taipei, Taiwan, October 2012, pp. 4.

[24] A. Vallan, A. Carullo, M. L. Casalicchio, A. Penna, G. Perrone, N. D. Vietro, A. Milella, and F. Fracassi, "A plasma modified fiber sensor for breath rate monitoring," in *Proc. IEEE Int. Symp. Med. Meas. Appl. (MeMeA)*, Lisbon, Portugal, June 2014, pp. 5.

[25] M. A. Zawawi, S. O'Keeffe, and E. Lewis, "Plastic Optical Fibre Sensor for Spine Bending Monitoring with Power Fluctuation Compensation," *Sensors*, vol. 13, no. 11, pp. 14466-14483, 2013.

[26] M. A. Zawawi, S. O'Keeffe, and E. Lewis, "Optical Fibre Bending Sensor With Automatic Intensity Compensation," *J. Lightw. Technol.*, vol. 33, no. 12, pp. 2492-2498, 2015.

[27] S. Dutta, A. Choudhury, and P. Nath, "Evanescent Wave Coupled Spectroscopic Sensing Using Smartphone," *IEEE Photon. Technol. Lett.*, vol. 26, no. 6, pp. 568-570, 2014.

[28] M. A. Hossain, J. Canning, S. Ast, P. J. Rutledge, T. L. Yen, and A. Jamalipour, "Lab-in-a-Phone: Smartphone-Based Portable Fluorometer for pH Measurements of Environmental Water," *IEEE Sensors J.*, vol. 15, no. 9, pp. 5095-5102, 2015.

[29] D. Gallegos, K. D. Long, H. Yu, P. P. Clark, Y. Lin, S. George, P. Natha, and B. T. Cunningham, "Label-free biodetection using a smartphone," *Lab on a Chip*, vol. 13, no. 11, pp. 2124-2132, 2013.

[30] Kort Bremer and Bernhard Roth, "Fibre optic surface plasmon resonance sensor system designed for smartphones," *Optics Express*, vol. 23, no. 13, pp. 17179-17184, 2015.

[31] A. Sultangazin, J. Kusmangaliyev, A. Aitkulov, D. Akilbekova, M. Olivero, and D. Tosi, "Design of a Smartphone Plastic Optical Fiber Chemical Sensor for Hydrogen Sulfide Detection," *IEEE Sensors J.*, vol. 17, no. 21, 2017.

[32] Daniele Tosi, Guido Perrone, and Alberto Vallan, "Performance Analysis of a Noncontact Plastic Fiber Optical Fiber Displacement Sensor with Compensation of Target Reflectivity," *J. Sensors*, vol. 2013, no. 1, pp. 12, 2013.

[33] Fiberfin.com, "Fiber and cable," 2018. [Online]. Available: https://store.fiberfin.com/index.php/products/fiber-and-cable.html. [Accessed: 14- Dec- 2018].

[34] Makeshaper.com, "How Much Does 3D Printer Filament Cost?" 2018. [Online]. Available: https://www.makeshaper.com/3d-printer-filament-price-cost/. [Accessed: 14- Dec- 2018].

Appendix A

A.1 Dependence of the received intensity on the displacement between fibers

The next part is the Matlab code for simulating the relationship between the reception of intensity and the displacement between the transmitting and receiving fibers according to Monte Carlo method.

```
d=0:5e-6:20000e-6;
M=100000;
NA=0.47;
G=3;
r_f=980e-6;
theta=asin(NA);
a=r_f/tan(theta);
theta_x=(rand(1,M)*2-1)*theta*2;
theta_y=(rand(1,M)*2-1)*theta*2;
p=theta_x.^2+theta_y.^2;%condition for propagation
r=ones(1,M);
r=r.*theta^2;
Accept=(p<r);%checking condition
theta_xA=theta_x(Accept);%counting how many photons can be
propagated
theta_yA=theta_y(Accept);
N=length(theta_xA);
for i=1:length(d)
    xh=(d(i)+a)*tan(theta_x);%coordinates of photons at
the receiving fiber
    yh=(d(i)+a)*tan(theta_y);
    Receive=((xh.^2+yh.^2)<(r_f.^2)  );%checking whether
photons hit the receiving fiber
    x_received= xh(Receive);
    y_received= yh(Receive);
    NR(i)=length(x_received);%counting the number of the
received photons
end
A=NR./N;
figure
plot(d*1e3, A,'LineWidth',4);
xlim([0 15]);
```

```
set(gca,'fontsize',29)
xlabel('Displacement (mm)','fontsize',29);
ylabel('Relative intensity','fontsize',29);
return
```

A.2 Android application

The following code is for the visual layout of the Android application:

```
<?xml version="1.0" encoding="utf-8"?>
<android.support.constraint.ConstraintLayout
xmlns:android="http://schemas.android.com/apk/res/android"
    xmlns:app="http://schemas.android.com/apk/res-auto"
    xmlns:tools="http://schemas.android.com/tools"
    android:layout_width="match_parent"
    android:layout_height="match_parent"
    tools:context=".MainActivity">

    <EditText
        android:id="@+id/editText"
        android:layout_width="0dp"
        android:layout_height="wrap_content"
        android:layout_marginLeft="16dp"
        android:hint="Click the button to proceed"
        android:inputType="textPersonName"
        app:layout_constraintLeft_toLeftOf="parent"
        app:layout_constraintRight_toLeftOf="@+id/button"
        android:layout_marginStart="16dp"
        app:layout_constraintBottom_toBottomOf="parent"
        android:layout_marginBottom="8dp" />

    <Button
        android:id="@+id/button"
        android:layout_width="wrap_content"
        android:layout_height="wrap_content"
        android:layout_marginLeft="16dp"
        android:layout_marginRight="16dp"
        android:onClick="sendMessage"
        android:text="Calculate"
        app:layout_constraintBaseline_toBaselineOf="@+id/editText"
        app:layout_constraintLeft_toRightOf="@+id/editText"
        app:layout_constraintRight_toRightOf="parent"
        android:layout_marginStart="16dp"
        android:layout_marginEnd="16dp" />

    <org.opencv.android.JavaCameraView
        android:id="@+id/camera_view"
        android:layout_width="wrap_content"
        android:layout_height="wrap_content"
        android:layout_marginLeft="8dp"
        app:layout_constraintLeft_toLeftOf="parent"
        android:layout_marginRight="8dp"
        app:layout_constraintRight_toRightOf="parent"
        app:layout_constraintHorizontal_bias="0.501"
```

```
        app:layout_constraintTop_toTopOf="parent"
        android:layout_marginTop="8dp"
        android:layout_marginBottom="32dp"
        app:layout_constraintBottom_toTopOf="@+id/editText" />

    <Button
        android:id="@+id/button4"
        android:layout_width="wrap_content"
        android:layout_height="wrap_content"
        android:layout_marginEnd="16dp"
        android:layout_marginRight="16dp"
        android:layout_marginBottom="8dp"
        android:onClick="stopThread"
        android:text="Stop"
        app:layout_constraintBottom_toTopOf="@+id/button"
        app:layout_constraintEnd_toEndOf="parent" />

</android.support.constraint.ConstraintLayout>
```

The next is the core code of the application:

```
package com.example.arman.testcamera;

import android.Manifest;
import android.content.pm.PackageManager;
import android.os.Environment;
import android.support.v4.app.ActivityCompat;
import android.support.v4.content.ContextCompat;
import android.support.v7.app.AppCompatActivity;
import android.os.Bundle;
import android.util.Log;
import android.view.SurfaceView;
import android.view.View;
import android.widget.EditText;
import org.opencv.android.BaseLoaderCallback;
import org.opencv.android.CameraBridgeViewBase;
import org.opencv.android.JavaCameraView;
import org.opencv.android.LoaderCallbackInterface;
import org.opencv.android.OpenCVLoader;
import org.opencv.core.Core;
import org.opencv.core.CvType;
import org.opencv.core.Mat;
import org.opencv.core.Scalar;
import java.io.File;
import java.io.FileOutputStream;
import java.io.IOException;
import java.io.OutputStreamWriter;

public class MainActivity extends AppCompatActivity implements
CameraBridgeViewBase.CvCameraViewListener2 {

    private static final String TAG = "OpenCVCamera";
    private JavaCameraView javaCameraView;
    Mat img;
    Scalar sop;//this variable is for saving the sum of pixels on a frame
    String line;
    Thread myThread;
```

```
    private BaseLoaderCallback baseLoaderCallback = new
BaseLoaderCallback(this) {
        @Override
        public void onManagerConnected(int status) {
            switch (status){
                case BaseLoaderCallback.SUCCESS:
                javaCameraView.enableView();//accessing native camera
                break;
                default:
                    super.onManagerConnected(status);
                    break;
            }
        }
    };

    @Override
    protected void onCreate(Bundle savedInstanceState) {
        super.onCreate(savedInstanceState);
        setContentView(R.layout.activity_main);//linking the application
with the visual layout

        if
(ContextCompat.checkSelfPermission(this,Manifest.permission.CAMERA)!=Packag
eManager.PERMISSION_GRANTED){
            ActivityCompat.requestPermissions(this,new
String[]{Manifest.permission.CAMERA}, 0);
        }
        javaCameraView=(JavaCameraView)findViewById(R.id.camera_view);
        javaCameraView.setVisibility(SurfaceView.VISIBLE);
        javaCameraView.setCvCameraViewListener(this);
    }

    @Override
    protected void onPause(){
        super.onPause();
        if (javaCameraView!=null){
            javaCameraView.disableView();
        }
    }

    @Override
    protected void onDestroy(){
        super.onDestroy();
        if (javaCameraView!=null){
            javaCameraView.disableView();
        }
    }

    @Override
    protected void onResume(){
        super.onResume();
        if (!OpenCVLoader.initDebug()){//activating OpenCV
            Log.d(TAG, "Opencv not loaded");
            OpenCVLoader.initAsync(OpenCVLoader.OPENCV_VERSION_3_3_0, this,
baseLoaderCallback);
        }
        else{
```

```
            Log.d(TAG, "Opencv loaded successfully");

baseLoaderCallback.onManagerConnected(LoaderCallbackInterface.SUCCESS);
        }
    }


    @Override
    public void onCameraViewStarted(int width, int height) {
        img = new Mat(height, width, CvType.CV_8UC4);//initializing the
storage for the camera image
    }

    @Override
    public void onCameraViewStopped() {
        img.release();
    }

    @Override
    public Mat onCameraFrame(CameraBridgeViewBase.CvCameraViewFrame
inputFrame) {
        javaCameraView.turnOnTheFlash();//activating the flashlight
        Mat img=inputFrame.gray();//converting the images to grayscale
        sop=Core.sumElems(img);//summing the pixels on a current frame
        line=""+sop.val[0];
        return img;
    }

    public void sendMessage (View view) {
        EditText editText = (EditText) findViewById(R.id.editText);
        editText.setText(line);

        (myThread = new Thread(new Runnable()
        {

            @Override
            public void run()
            {
                while (!Thread.interrupted())
                    try
                    {
                        Thread.sleep(50);
                        runOnUiThread(new Runnable()
                        {

                            @Override
                            public void run()
                            {
                                writeToFile(line);
                            }
                        });
                    }
                    catch (InterruptedException e)
                    {
                    }
            }
        })).start();
    }
```

```
    public void stopThread (View view){
        myThread.interrupt();
    }

    public void writeToFile(String data)
    {
        final File path =//creating a directory for storing the sums of
pixels
                Environment.getExternalStoragePublicDirectory
                        (
                                Environment.DIRECTORY_DCIM + "/YourFolder/"
                        );

        if(!path.exists())
        {
            path.mkdirs();
        }

        final File file = new File(path, "sums_of_pixels.txt");//saving the
sums of pixels to a file

        try
        {
            file.createNewFile();
            FileOutputStream fOut = new FileOutputStream(file, true);
            OutputStreamWriter myOutWriter = new OutputStreamWriter(fOut);
            myOutWriter.append(data);
            myOutWriter.append("\n");

            myOutWriter.close();

            fOut.flush();
            fOut.close();
        }
        catch (IOException e)
        {
            Log.e("Exception", "File saving failed: " + e.toString());
        }
    }
}
```

Appendix B

B.1 Representation of the measurements from the displacement modulation

The following code is for plotting the dependence of the intensity values on the respective displacements between the transmitting and receiving fibers as captured by the camera.

```
intensity=zeros(1,17);
for i=1:17
    j=i-1;
    name=sprintf('mm_noadjustment/mm_%d.jpg',j);%importing
the images received by the camera at 0-16 mm displacements
    A=imread(name);
    B=rgb2gray(A);
    intensity(i)=sum(sum(B));%finding the sum of pixels on
the image
end
d=0:1:16;
intensity_max=intensity(1);
intensity=intensity/intensity_max;
plot(d,intensity,'LineWidth',4)
hold on
plot(d(7),intensity(7),'-
s','MarkerSize',10,'MarkerEdgeColor','red','MarkerFaceColo
r',[1 .6 .6])
plot(d(2),intensity(2),'-
s','MarkerSize',10,'MarkerEdgeColor','red','MarkerFaceColo
r',[1 .6 .6])
plot(d(13),intensity(13),'-
s','MarkerSize',10,'MarkerEdgeColor','red','MarkerFaceColo
r',[1 .6 .6])
hold off
set(gca,'fontsize',29)
xlabel('Displacement (mm)','fontsize',29);
ylabel('Relative intensity','fontsize',29);
```

B.2 Processing the measurements of breathing

The next code is for the experimental part. The video was captured by the camera over 30 seconds during breathing. Then, each frame of the video was saved as an image and imported to Matlab. Hence, the changes in breathing activity were processed. The measurements were taken 5 times.

```
fr=707;%707 frames with capturing rate of 23.56 fps
correspond to a period of 30 seconds
POF_intensities=zeros(1,fr);
n=2828;
POF_fft=zeros(1,n);
for i=1:fr
    name=sprintf('1mm_frames/frames
(%d).jpg',i);%importing the images from the camera
    A=imread(name);
    B=rgb2gray(A);
    POF_intensities(i)=sum(sum(B));%finding the sum of
pixels on each image
end
POF_intensities=detrend(POF_intensities);%removing DC
value
intensity_max=POF_intensities(1);
POF_intensities=POF_intensities/intensity_max;
[b a]=butter(2,[0.02 0.09],'bandpass');%Butterworth filter
POF_intensities=filter(b,a,POF_intensities);
T=1/23.56;
t=0:T:30.00848896;
Fs=1/T;%sampling frequency
f=Fs*(0:(n/2))/n;
POF_fft=abs(fft(POF_intensities,n)/n);%applying FFT
figure%plotting the filtered signal in time domain
plot(t,POF_intensities,'LineWidth',2)
xlabel('Time (s)');
ylabel('Relative intensity');
set(gca,'fontsize',25);
figure%plotting the frequency components of the signal
plot(f,POF_fft(1:n/2+1),'LineWidth',2)
xlim([0 2])
xlabel('Frequency (Hz)');
ylabel('Spectral density');
set(gca,'fontsize',25);
```

B.3 Processing the measurements done by the sensor and the accelerometer

The next part is the code for comparing breathing intensities obtained by the accelerometer and the POF-based sensor.

```
acc=xlsread('accelerometer1.xlsx','B:B');%loading the acceleration values obtained by the accelerometer during breathing
acc=detrend(acc);%removing DC value from the accelerometer signal
acc_max=acc(1);
acc=acc./acc_max;
[c d]=butter(2,[0.005 0.015],'bandpass');%filtering by the Butterworth filter
acc=filter(c,d,acc);
m=6000;
Tb=1/100;
tb=0:Tb:32.18;%measuring period
Fsb=1/Tb;%sampling rate of the acceleromter
acc_FFT=abs(fft(acc,m)/m);%applying FFT to the accelerometer signal
fb=Fsb*(0:(m/2))/m;
plot(fb,acc_FFT(1:m/2+1),'LineWidth',2)
xlim([0 2]);
hold on
%the video was captured by the camera when using the POF-sensor
%then, each frame of this video was saved as a separate image file
fr=497;%the resulting number of frames over 30 seconds (the camera rate is 16.57 frames per second)
pof_intensities=zeros(1,fr);
n=1988;
for i=1:fr
    name=sprintf('POF_measurements1/frame (%d).jpg',i);%importing the frames of the captured video
    A=imread(name);
    B=rgb2gray(A);
    pof_intensities(i)=sum(sum(B));
end
pof_intensities=detrend(pof_intensities);%removing the DC value from the signal captured by the POF-sensor
intensity_max=pof_intensities(1);
```

```
pof_intensities=pof_intensities/intensity_max;
[b a]=butter(2,[0.02 0.09],'bandpass');%Butterworth filter
pof_intensities=filter(b,a,pof_intensities);
T=1/16.57;
t=0:T:29.93361497;
Fs=1/T;
f=Fs*(0:(n/2))/n;
POF_fft=abs(fft(pof_intensities,n)/n);%FFT transform
plot(f,POF_fft(1:n/2+1),'LineWidth',2)
xlim([0 2])
set(gca,'fontsize',29)
ylabel('Spectral density','fontsize',29);
xlabel('Frequency (Hz)','fontsize',29);
lgd=legend('Reference','Sensor');
lgd.FontSize=29;
hold off
```

B.4 Processing the measurements collected by the Android application

The following code is for extracting the breathing rate from the intensities collected by the Android application. The application captures the sums of pixels on the frame instead of saving the frame itself. These sums are saved to the text file. It is exported to Matlab for further processing.

```
POF_sums=xlsread('application_measurements.xlsx','A:A');%t
he sum values are imported to Matlab
%the sums were captured over a period of 30 seconds
POF_sums=POF_sums(1:601);
POF_sums=detrend(POF_sums);%removing DC value
POF_sum_max=POF_sums(1);
POF_sums=POF_sums/POF_sum_max;
[b a]=butter(2,[0.02 0.09],'bandpass');%Butterworth filter
POF_sums=filter(b,a,POF_sums);
T=50*10^(-3);
Fs=1/T;%sampling frequency of the Android application
t=0:T:600*T;
POF_sums_FFT=fft(POF_sums);%FFT
POF_sums_FFT=2*POF_sums_FFT(1:ceil((length(POF_sums)+1)/2)
);
f=0:Fs/length(POF_sums):Fs/2;
```

```
POF_sums_FFT = POF_sums_FFT/(2*length(f));
acc_sums=xlsread('accelerometer2.xlsx','A:A');%importing
data from accelerometer
acc_sums=acc_sums(1001:4001);
acc_sums=detrend(acc_sums);
acc_max=acc_sums(1);
acc_sums=acc_sums/acc_max;
[b a]=butter(2,[0.005 0.015],'bandpass');
acc_sums=filter(b,a,acc_sums);
T_acc=1/100;
acc_fft=fft(acc_sums);
acc_fft=2*acc_fft(1:ceil((length(acc_sums)+1)/2));
Fs_acc=1/T_acc;%sampling rate of accelerometer; 100fps
f_acc=0:Fs_acc/length(acc_sums):Fs_acc/2;
acc_fft=acc_fft/(2*length(f_acc));
figure
plot(f,abs(POF_sums_FFT),'LineWidth',2)
hold on
plot(f_acc,abs(acc_fft),'LineWidth',2)
lgd=legend('Sensor','Reference');
lgd.FontSize=29;
xlim([0 2])
set(gca,'fontsize',29)
ylabel('Spectral density','fontsize',29);
xlabel('Frequency (Hz)','fontsize',29);
```

Appendix C

Table C.1 was used to calculate the relative losses in Table 4.2.

Table C.1: Sum of pixels calculated for 3 multiplexed fibers

Bent fiber	State	Recorded intensity (sum of pixels)		
		1st fiber	2nd fiber	3rd fiber
1st fiber	Default state	2.89E+07	4.24E+07	2.67E+07
	1st fiber is bent	2.58E+07	4.20E+07	2.62E+07
2nd fiber	Default state	2.88E+07	4.20E+07	2.61E+07
	2nd fiber is bent	2.67E+07	3.96E+07	2.48E+07
3rd fiber	Default state	2.63E+07	4.19E+07	2.68E+07
	3rd fiber is bent	2.59E+07	4.12E+07	2.54E+07

Table C.2 was used to calculate the relative losses in Table 4.4.

Table C.2: Sum of pixels found when multiplexing 3 cut fibers

Bending angle	State	Recorded intensity (sum of pixels)		
		1st fiber	2nd fiber	3rd fiber
10°	Default state	7.14E+06	1.74E+07	7.37E+06
	1st fiber is bent	6.22E+06	1.79E+07	6.73E+06
	2nd fiber is bent	7.03E+06	1.81E+07	6.87E+06
	3rd fiber is bent	4.20E+06	1.52E+07	4.63E+06
20°	Default state	1.35E+07	2.84E+07	1.13E+07
	1st fiber is bent	7.97E+06	3.06E+07	1.15E+07
	2nd fiber is bent	1.39E+07	2.05E+07	1.07E+07
	3rd fiber is bent	1.23E+07	2.83E+07	1.08E+07

Table C.3 was used to calculate the relative losses in Table 4.6.

Table C.3: Sum of pixels found when multiplexing 2 cut fibers

State	Recorded intensity (sum of pixels)	
	1st fiber	2nd fiber
Default state	2.11E+06	9.65E+05
1st fiber is bent	1.45E+06	9.11E+05
2nd fiber is bent	1.92E+06	7.71E+05